ISSN 2658-3518

LIMNOLOGY & FRESHWATER BIOLOGY

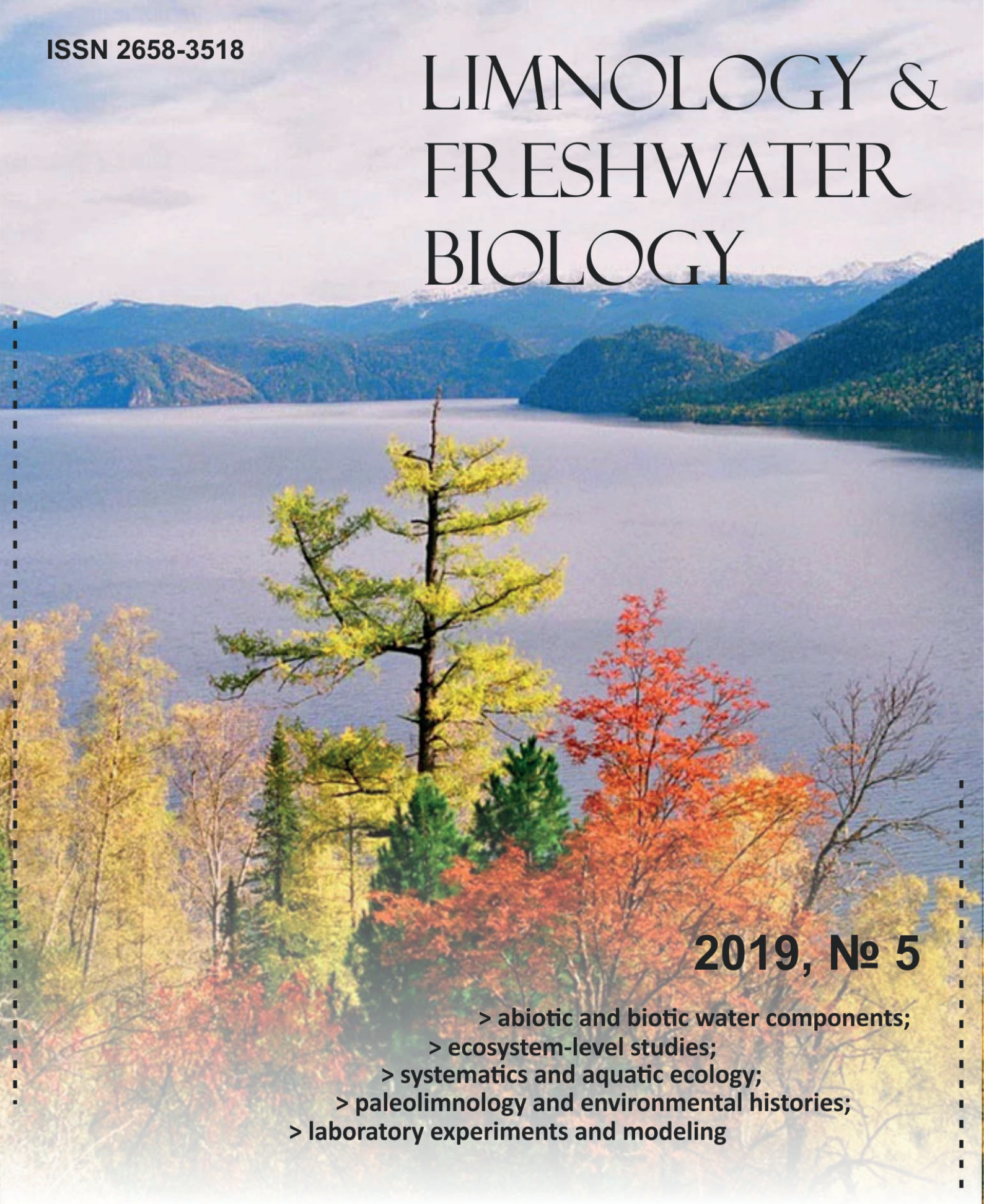

2019, № 5

> abiotic and biotic water components;
> ecosystem-level studies;
> systematics and aquatic ecology;
> paleolimnology and environmental histories;
> laboratory experiments and modeling

Limnology and Freshwater Biology 2019 (5): 286-296 DOI:10.31951/2658-3518-2019-A-5-286

Original Article

ISSN 2658-3518
LIMNOLOGY FRESHWATER BIOLOGY
www.limnolfwbiol.com

Changes in lipid composition and lipid peroxidation products content in the freshwater mussel *Anodonta cygnea* L. under cadmium effect

Fokina N.N.*, Vasil'eva O.B., Ruokolainen T.R., Nemova N.N.

Institute of Biology of Karelian Research Centre of Russian Academy of Sciences, Pushkinskaja St. 11, 185 910 Petrozavodsk, Russia

ABSTRACT. In order to identify specific biomarkers to cadmium-induced oxidative stress in freshwater organisms, changes in the composition of membrane and storage lipids and their fatty acids in the gills and digestive glands of freshwater mussels, *Anodonta cygnea* (Linnaeus, 1758), exposed to cadmium ions at 10, 50 and 100 μg/L were studied. Cadmium-induced oxidative stress was estimated by the content of lipid peroxidation products such as conjugated dienes and trienes, malondialdehyde, and Schiff bases. Accumulation of lipid peroxidation products in the gills and digestive glands reflected the intensity of lipid peroxidation, depending on the concentration and duration of cadmium exposure. Changes in the fatty acid composition of phospholipids and triacylglycerols reflected their compensatory role in the response of the mussels to the action of cadmium at various concentrations. Some indices of lipid composition (phosphatidylserine and triacylglycerol content) similarly altered under cadmium effect in both marine and freshwater mussels. The assessment of oxidative stress biomarkers and the main targets for these oxidative processes including lipids and their fatty acid composition makes it possible to identify protective biochemical mechanisms providing the high resistance of mussels to environmental pollution.

Keywords: phospholipids, fatty acids, malondialdehyde, metal, toxicity, bivalves

1. Introduction

Mussels are used as sentinel organisms in monitoring studies of aquatic ecosystems, as well as in ecological and toxicological studies of the effects of metal accumulation on the health of organisms (Perceval et al., 2002; Wadige et al., 2014). Assessment of cadmium effects on the vitality of organisms exists for both marine and freshwater mussels (Geret et al., 2002; Perceval et al., 2002; Wadige et al., 2014). A wide range of the mussels responses to cadmium has been shown: enzyme inhibition and injury to cell membranes (Chelomin et al., 1998), apoptosis induction (Xia et al., 2016), and neurotoxicity (Méndez-Armenta and Ríos, 2007). Metals with variable oxidation states may disrupt biological membrane composition, initiating lipid peroxidation (LPO) by Fenton reactions (Valko et al., 2005; Oxidative stress..., 2011). Cadmium ions and their chelate complexes cannot take part in the formation of reactive oxygen species through such redox processes but suppress the activity of antioxidant enzymes, provoking the unregulated formation of reactive oxygen species and eventually inducing peroxidation of polyunsaturated fatty acids in membrane phospholipids (Viarengo et al., 1990; Regoli et al., 1998; Geret et al., 2002; Valko et al., 2005; Oxidative stress..., 2011; Repetto et al., 2012). In ecological and toxicological studies, to assess the intensity of LPO, the concentration of malondialdehyde (MDA) is used as a marker of oxidative stress (e.g., Oxidative stress..., 2011). LPO is accompanied by the formation of a wide range of intermediate products possessing toxic effects on the organism and damaging the composition of lipoproteins, proteins and nucleic acids (Waller and Recknagel, 1977). The composition of the intermediate LPO products is determined by the membrane lipid composition exposed to oxidative stress (Sevanian and Hochstein, 1985; Gutteridge and Halliwell, 1990). Thus, conjugated dienes (CoD) are the primary LPO products of polyunsaturated fatty acids (PUFA) and contain 3 or more double bonds (termed highly unsaturated fatty acids, HUFA). MDA is a common product of the lipid hydroperoxide decomposition of HUFA. Conjugated trienes (CoT) are formed from CoD and possess stronger cytotoxic effects than diene conjugates (Suzuki et al., 2001). The product of the interaction of MDA and the amino groups of phospholipids and proteins are Schiff bases (SchB). SchB constitutes molecular crosslinks with membrane components (mainly proteins) disrupting in cell membranes (Traverso et al., 2004).

Changes in lipid composition of mussels have been shown as an effect of cadmium exposure (Fokina et al., 2013; Merad et al., 2017). Along with LPO products, lipid and fatty acid composition can serve as biomarkers reflecting the toxic

*Corresponding author.
E-mail address: fokinann@gmail.com (N.N. Fokina)

effects of metals on organism health status (Gladyshev et al., 2012; Fokina et al., 2013; Perrat et al., 2013; Merad et al., 2017). For example, the accumulation of neutral lipids, including triacylglycerols, in the digestive glands of mussels is a biomarker for environmental contamination, and it indicates the activation of autophagy processes (Moore et al., 2007). However, the regulation of lipid composition seems to be a compensatory mechanism to prevent non-selective membrane permeability to ions by the adverse effects of oxidative stress (Gladyshev et al., 2012; Fokina et al., 2013). In particular, increases in cholesterol and oleic acid contents, which probably contribute to the stabilization of membrane permeability and metal detoxification under the impact of copper, were shown in the marine mussels, *Mytilus edulis* L. (Fokina et al., 2013). In the studies of the metal-induced oxidative stress effects on organism health, it is recommended to evaluate not only changes in LPO products but also changes in its substrates, i.e., in lipid and fatty acid composition. Thus, the study of the lipid and fatty acid composition (triacylglycerols, sterols and phospholipid fractions) and LPO products (conjugated dienes and trienes, malondialdehyde and Schiff bases) in the gills and digestive glands of freshwater mussels, *Anodonta cygnea* (Linnaeus, 1758), is required to identify the biomarkers reflecting the cadmium effect.

2. Materials and methods

2.1. Experiment design

Adult freshwater mussels, *Anodonta cygnea* (Linnaeus, 1758), were collected from the Suna River (Republic of Karelia, Russia). The mussel samples were taken from a riverbed historically isolated from sources of industrial pollution. Our results of the whole body mussel tissues analysis by inductively coupled plasma mass spectrometry (XSeries-2 ICP-MS, Thermo Fisher Scientific, Waltham, MA, USA) showed that cadmium content in the mussels was 0.9 mg/kg. In particular, it was shown that mussels from urban localities contain 3.9 to 4.6 mg/kg cadmium compared to mussels from rural areas, which contain 0.4-3.2 mg/kg of cadmium (Manly and George, 1977). Shell length was 71.7 ± 3.8 mm. Total weight of mussels (soft tissues+mantle fluid+shell) was 34.5 ± 5.9 g. The experiments were conducted at the Aquarium Complex of the Institute. The mussels were acclimated to laboratory conditions for seven days in 5 L Plexiglas® aquariums containing dechlorinated water, with a 12/12 photoperiod and constant aeration (4 mussels per aquarium). The physical and chemical parameters of the aquarium water were monitored. The temperature was 22 ± 1.0 °C, pH = 7.4 ± 0.03, dissolved oxygen (DO) 8.3 ± 0.5 mg/L, total mineralisation 11.8 ± 1.6 mg/L, total water hardness 0.5 - 0.85 mmol/L, NH_4^+ 1.5 ± 0.5 mg/L, NO_2^- 0.0 mg/L, NO_3^- 1.2 ± 1.2 mg/L, SO_4^{2-} 14.2 ± 0.3 mg/L, and Cl^- 3.2 ± 0.9 mg/L. The water was replaced twice a day.

After acclimation, the mussels were divided into eight groups of 4 mussels each: the control was exposed to dechlorinated water (two aquariums), and three experimental groups were exposed to 10, 50, and 100 µg/L of cadmium (two aquariums for each experimental group). A stock solution of cadmium was prepared by dissolving cadmium (II) chloride in distilled water to a Cd^{2+} concentration of 20 mg/L. The aquarium water was renewed twice a day and further the calculated amount of cadmium stock solution was added in aquarium water after each water change. During the experiment, the water temperature, pH, DO, total mineralisation, total water hardness and anion content were monitored and kept stable (means ± SD): 21 ± 1.0 °C, 7.0 ± 0.1, 7.8 ± 0.5 mg/L, 11.8 ± 1.4 mg/L, 0.5 - 0.85 mmol/L, NH_4^+ 1.7 ± 0.4 mg/L, NO_2^- 0.09 ± 0.03 mg/L, NO_3^- 2.5 ± 0.0 mg/L, SO_4^{2-} 14.2 ± 0.5 mg/L, and Cl^- 4.2 ± 0.4 mg/L. After every 24-hour experimental exposure of mussels, aquarium water was taken to analyze its cation composition (Fig. 1) by inductively coupled plasma mass spectrometry (XSeries-2 ICP-MS, Thermo Fisher Scientific, Waltham, MA, USA) (Slukovskii et al., 2017).

At the end of the experiment (one and three days), the soft tissues of *A. cygnea* (gills and digestive glands, n=4, from each experimental treatment group) were fixed for further biochemical analysis. Until the lipid analysis, the tissues were stored in 96 % ethanol at 4 °C. Tissues for lipid peroxidation products and cation composition measurements were stored at - 80 °C. Frozen soft tissues for cation composition were freeze dried for 24 hours (FreeZone, Labconco, Kansas City, MO, USA) and analyzed by ICP-MS.

2.2. Biochemical analysis

Biochemical analyses of the lipid peroxidation products and the lipid profiles in the gills and digestive glands of the freshwater mussels, *A. cygnea*, were conducted in the Equipment Sharing Centre of the Karelian Research Centre of the Russian Academy of Sciences (Petrozavodsk, Russia).

Analysis of total lipid composition

Lipids were extracted with chloroform/methanol (2:1, v/v) according to Folch et al. (1957). The extracted lipids were spotted onto silica gel thin-layer chromatography plates (TLC Silica gel 60 F254 plates, "Merck", Germany) and separated into different fractions of lipid classes using petroleum ether/diethyl ether/acetic acid (90:10:1, v/v) as the mobile phase. The identification of the fractions was performed using standards: phospholipid mixture (P3817 "Supelco", USA), cholesterol (C8667 "Sigma", USA), glyceryl trioleate (92860 "Sigma", USA) and cholesteryl palmitate (C78607 "Aldrich", USA). The quantitative composition of the fractions was measured at 540 nm wavelength for phospholipids, triacylglycerols and sterol esters and 550 nm wavelength for the sterol fraction using an SF-2000 UV/Vis spectrophotometer (Saint-Petersburg, Russia) (Sidorov et al., 1972; Engelbrecht et al., 1974).

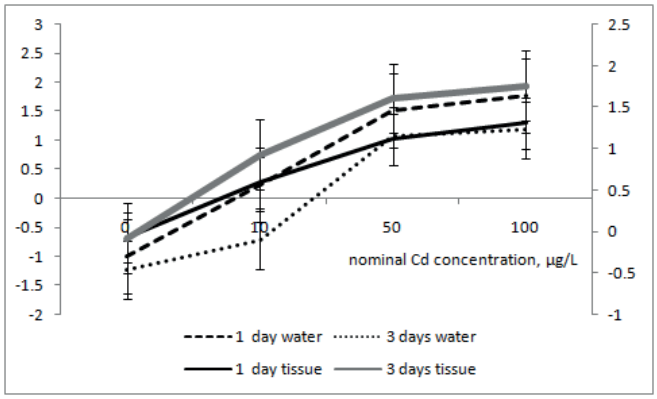

Fig. 1. Cadmium concentration (log10-transformed) in aquarium water (µg/L) and mussel tissues (µg/g dry weight).

Phospholipid fractions determination

The composition of phospholipid fractions (phosphatidylinositol (PI), phosphatidylserine (PS), phosphatidylethanolamine (PE), phosphatidylcholine (PC), lysophosphatidylcholine (LPC) and sphingomyelin (SM)) was determined by high-performance liquid chromatography using the method of Arduini et al. (1996) on a Nucleosil 100-7 column ("Elsiko", Russia) with the liquid phase acetonitrile/ hexane/methanol/phosphorus acid (918:30:30:17.5, v/v) and UV-spectrophotometer at a 206 nm wavelength using liquid chromatography from "Aquilon. Stayer" (Moscow, Russia). Peaks were identified by reference to the retention times of the authentic standards: phospholipid mixture (P3817 "Supelco", USA), phosphatidylserine (P7769, "Sigma", USA) and sphingomyelin (S7004, "Sigma", USA).

Analysis of fatty acid composition in phospholipids and triacylglycerols

The total phospholipids and triacylglycerols fractions were separated from the total lipids using thin-layer chromatography on TLC Silica gel 60 F254 plates ("Merck", Germany). Fatty acid methyl esters (FAME) from the fractions were prepared using methanol and acetyl chloride. The separation of FAME was in an "Agilent 7890A" gas-liquid chromatograph ("Agilent Technologies", USA) with a flame ionization detector using "DB-23" columns (60 m – 0.25 mm) ("Agilent Technologies", USA) and nitrogen as the mobile phase. FAMEs were identified by comparison with standard mixes ("Supelco", USA). The degree of unsaturation of the phospholipids and triacylglycerols was estimated using an unsaturation index (UI), which was calculated as UI = (%monoenoic FA + 2•%dienoic FA + 3•%trienoicFA + 4•%tetraenoicFA + 5•%pentaenoicFA + 6•%hexaenoicFA)/ Σsaturated FA (Pirini et al., 2007).

Analysis of lipid peroxidation products

Conjugated dienes (CoD) were analysed in lipid extract prepared by Folch et al. (1957) method. An aliquot of the lipid extract was redissolved in a methanol/pentane mixture (5:1, v/v) and was measured at 233 nm ($\varepsilon = 2.1\times10^4$ M^{-1} cm^{-1}). CoD level was expressed in nmol/g of wet tissue (Gavrilov et al., 1987). Malondialdehyde (MDA) was measured by the thiobarbituric acid reactive species method (Ohkawa et al., 1979; Bird and Draper, 1984) by adding of 0.2 mL of tissue homogenate to 1.5 mL of 20 % orthophosphoric acid (pH 3.5) and 1.5 mL of 0.8 % thiobarbituric acid. Then, samples were heated in a 95 °C water bath for 1 h. After cooling, 1.0 mL chilled water and 5.0 mL butanol-pyridine mixture (15:1, v/v) were added. Samples were vortexed for 15 s. The flocculent precipitate was removed by centrifugation at 3000 g for 10 min. Homogenate absorbance was measured at 532 nm using 1,1,3,3-tetra-ethoxy-propane as a reference. The MDA level was expressed in nmol/g of wet tissue. Schiff bases (SchB) and conjugated trienes (CoT) were extracted by mixture heptanes/isopropanol (3:7, v/v). The heptane layer was measured at 220 nm (isolated double bonds), 278 nm (CoT) and 400 nm (SchB). The concentrations of CoT and SchB were evaluated by the 278/220 and 400/220 ratios and expressed as relative units (Hyshiktuyev et al., 1996).

Statistical analysis

Statistical analyses were performed with StatSoft Statistica v 7.0. Kolmogorov-Smirnov and Lilliefors tests were used to examine the normality of the distribution of the investigated parameters. Homogeneity of variance was assessed using Levene's test. As the distribution of all data deviated from the normal range, the significance of the differences was tested by non-parametric statistics. The Mann–Whitney U and Kruskal-Wallis tests were performed to test the differences in the studied biochemical indices, depending on the dose and duration of cadmium effect. The differences were considered significant at $p < 0.05$. The correlation of the changes in the biochemical parameters and dose-duration effects was estimated by the Spearman's rank correlation coefficients (Hill and Lewicki, 2007). The results of the lipid peroxidation products are presented in the form of the mean values ± the standard deviation. The results of the lipid composition are presented as the mean values ± the standard error.

3. Results

3.1. Lipid composition

Gills

In the first experimental day at 50 μg/L and 100 μg/L of cadmium increased, sterol content was observed, and decreased LPC content was verified in the gills of *A. cygnea* (Fig. 2, Fig. 3). Further exposure (3 days) of the mussels to 100 μg/L cadmium resulted in a decrease in the content of the total phospholipids and their fractions (phosphatidylinositol, phosphatidylserine, sphingomyelin, phosphatidylethanolamine, phosphatidylcholine and its lysoform). The effect of 10 μg/L cadmium caused a decrease in the LPC content on the third day of the experiment. In addition, on the third experimental day under all studied cadmium doses, there was a decrease in TAG content in the gills (Fig. 2).

Figures 4-6 show that on the first day of the experiment under all studied cadmium doses, the saturated fatty acid content (mainly palmitic acid, 16:0) increased, and the content of monounsaturated fatty acids (primarily 20:1 acids) and n-6 PUFAs (linoleic 18:2n-6 and arachidonic 20:4n-6 acids) decreased in the gill phospholipids. At the same time, there was a decrease in the unsaturation index of the phospholipid fatty acid composition (Fig. 7). On the first experimental day, increased contents of saturated acids (20:0 and 22:0), as well as a decreased arachidonic 20:4n-6 acid content, were observed in the gill triacylglycerols (Fig. 5, Fig. 6). In contrast to the first experimental day, on the third day, the saturated fatty acid content in gill phospholipids and triacylglycerols decreased, while the content of PUFAs, predominantly the n-6 family, increased, causing a significant increase in the unsaturation index of the phospholipids and triacylglycerol fatty acids (Fig. 4-Fig. 7).

Digestive glands

In the digestive glands of *A. cygnea*, an increase in the phospholipid proportion, mainly the dominant membrane phospholipid - phosphatidylcholine (PC), was detected on the first day in 10 and 100 μg/L cadmium (Fig. 2, Fig. 3). There was an increase in the content of sterols (10 and 100 μg/L cadmium) and triacylglycerols (100 μg/L cadmium). On the first experimental day under 100 μg/L cadmium, a decrease in the phosphatidylserine (PS) content was observed that subsequently (on the third experiment day) significantly increased under all studied cadmium doses (10, 50 and 100 μg/L). An accumulation of triacylglycerols (TAG) in the digestive glands was also noted on the third experimental

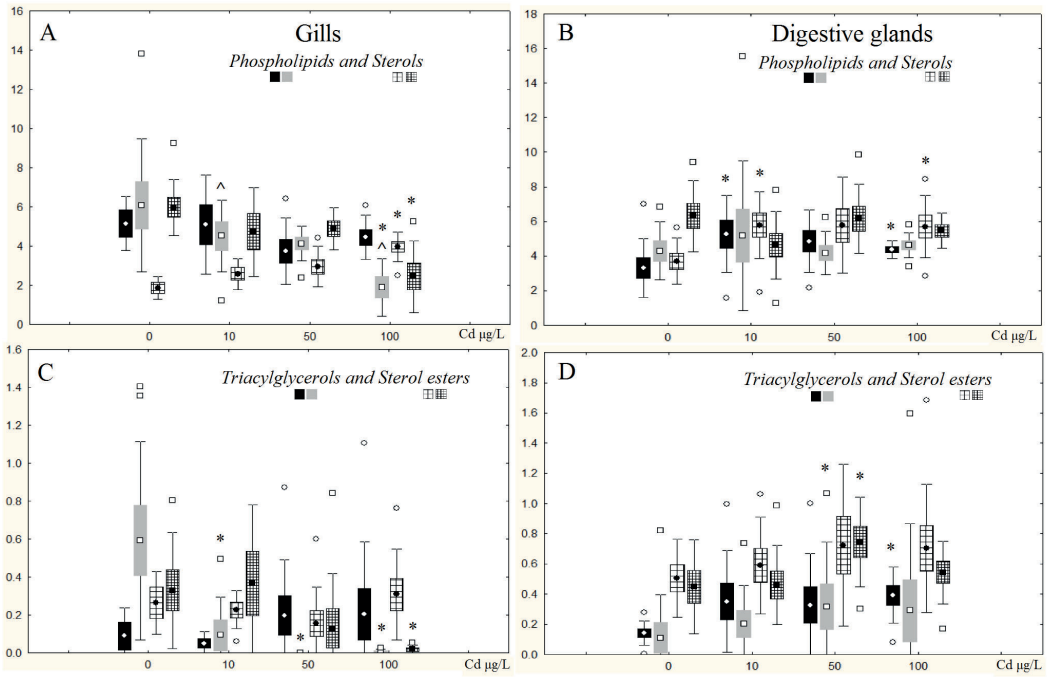

Fig. 2. Lipid classes content (% dry weight) in gills (A and C) and digestive glands (B and D) of freshwater mussels *A. cygnea* under cadmium effects: black columns and columns in large cells – 1 day exposure; grey columns and columns in small cells – 3 days exposure. Values are means ± standard error (N = 7): * – significant differences in comparison with the control (Mann-Whitney test, $P < 0.05$); ^- significant differences compared to the cadmium concentrations (Kruskal-Wallis test, $P < 0.05$).

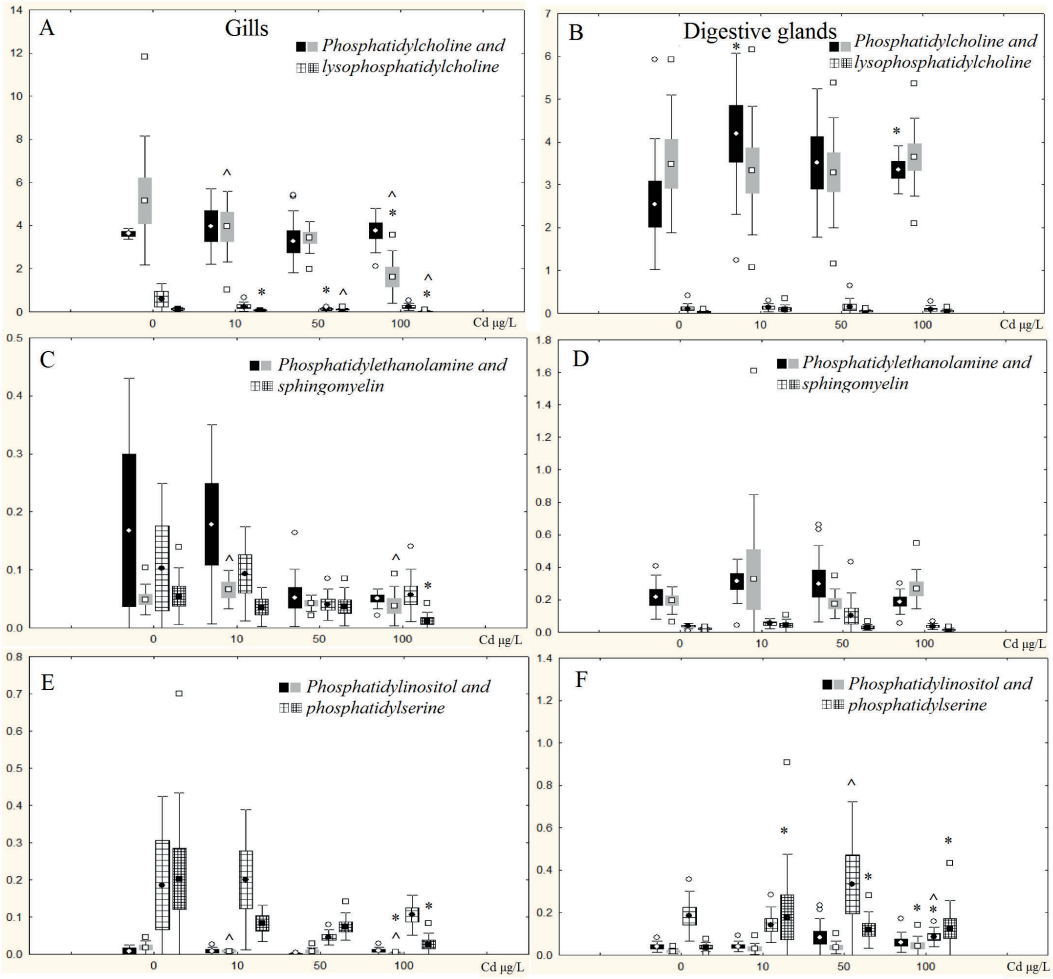

Fig. 3. Phospholipid classes content (% dry weight) in gills (A, C and E) and digestive glands (B, D and F) of freshwater mussels *A. cygnea* under cadmium effects: black columns and columns in large cells – 1 day exposure; grey columns and columns in small cells – 3 days exposure. Values are means ± standard error (N = 7): * – significant differences in comparison with the control (Mann-Whitney test, $P < 0.05$); ^- significant differences compared to the cadmium concentrations (Kruskal-Wallis test, $P < 0.05$).

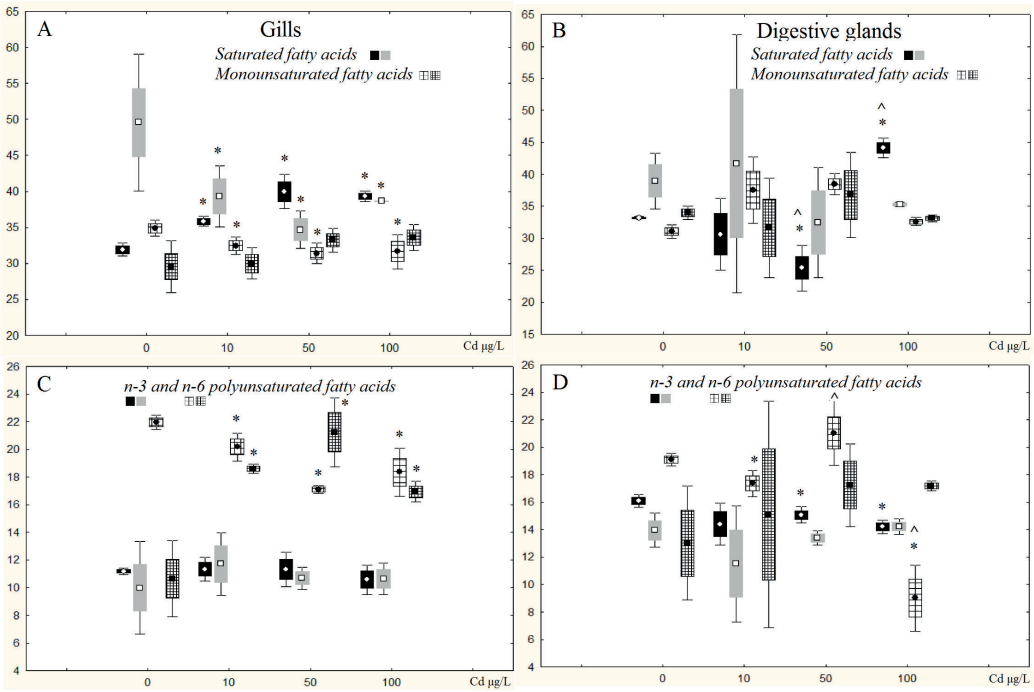

Fig. 4. Phospholipid fatty acid composition (% sum fatty acids) of gills (A and C) and digestive glands (B and D) in freshwater mussels *A. cygnea* under cadmium effects: black columns and columns in large cells – 1 day exposure; grey columns and columns in small cells – 3 days exposure. Values are means ± standard error (N = 7): * – significant differences in comparison with the control (Mann-Whitney test, $P < 0.05$); ^- significant differences compared to the cadmium concentrations (Kruskal-Wallis test, $P < 0.05$).

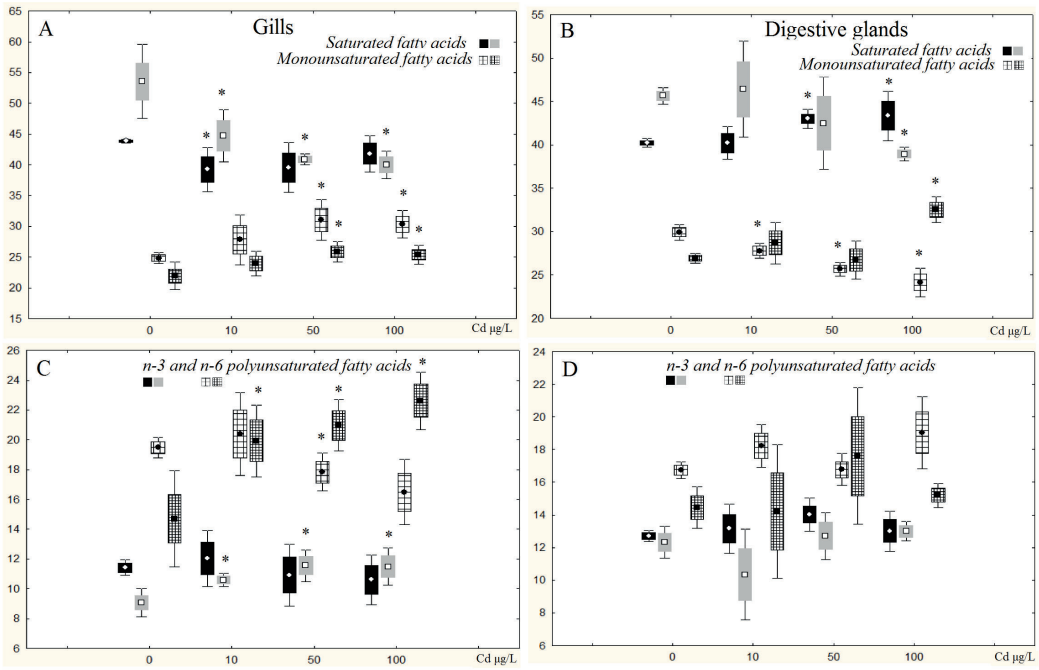

Fig. 5. Triacylglycerols fatty acid composition (% sum fatty acids) of gills (A and C) and digestive glands (B and D) in freshwater mussels *A. cygnea* under cadmium effects: black columns and columns in large cells – 1 day exposure; grey columns and columns in small cells – 3 days exposure. Values are means ± standard error (N = 7): * – significant differences in comparison with the control (Mann-Whitney test, $P < 0.05$); ^- significant differences compared to the cadmium concentrations (Kruskal-Wallis test, $P < 0.05$).

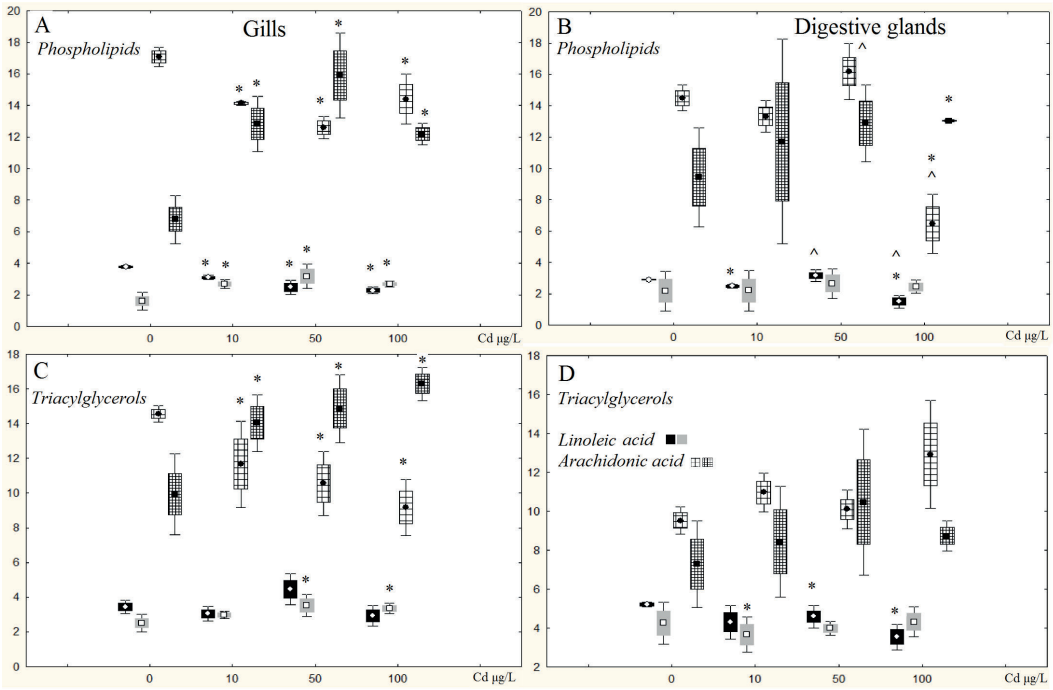

Fig. 6. Content of linoleic acid and arachidonic acid (% sum fatty acids) in phospholipids (A and B) and triacylglycerols (C and D) of gill (A and C) and digestive glands (B and D) in freshwater mussels *A. cygnea* under cadmium effects: black columns and columns in large cells – 1 day exposure; grey columns and columns in small cells – 3 days exposure. Values are means ± standard error (N = 7): * – significant differences in comparison with the control (Mann-Whitney test, $P < 0.05$); ^ - significant differences compared to the cadmium concentrations (Kruskal-Wallis test, $P < 0.05$).

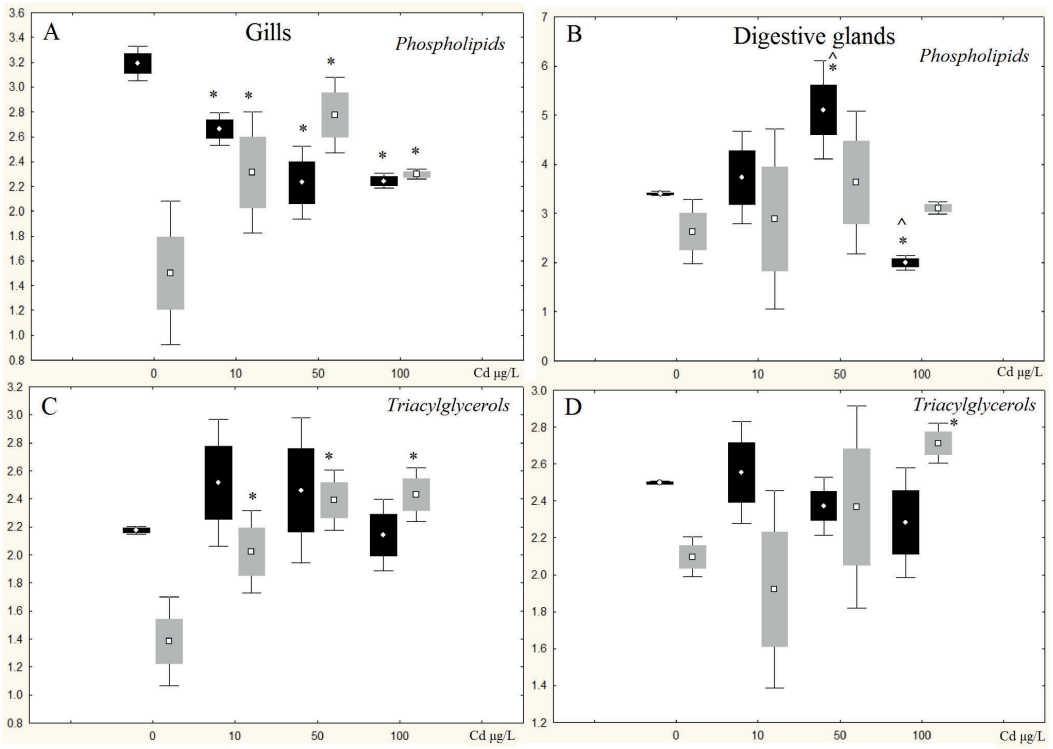

Fig. 7. Unsaturation index of phospholipids (A and B) and triacylglycerols (C and D) in gills (A and C) and digestive glands (B and D) of freshwater mussels *A. cygnea* under cadmium effects: black columns – 1 day exposure; grey columns – 3 days exposure. Values are means ± standard error (N = 7): * – significant differences in comparison with the control (Mann-Whitney test, $P < 0.05$); ^- significant differences compared to the cadmium concentrations (Kruskal-Wallis test, $P < 0.05$).

day (under 50 μg/L cadmium). On the first experimental day, changes in the fatty acid composition of the digestive gland phospholipids were determined by the cadmium concentrations (Fig. 4, Fig. 7). Thus, modifications in the fatty acid composition similar to those in the gills on the third day were observed under 50 μg/L cadmium (reduced saturated fatty acid content and increased unsaturation index). At the same time, under 100 μg/L cadmium, an increase in saturated fatty acid content and a decrease in the index of unsaturation were observed (these modifications were noted in the gills on the first experimental day). The fatty acid composition of the triacylglycerols significantly changed under 50 and 100 μg/L cadmium (Fig. 5). Unlike the fatty acid composition of phospholipids, they did not depend on the cadmium concentration. On the first experimental day, there was an increase in the saturated fatty acid content (mainly palmitic acid 16:0) and a decrease in the unsaturated fatty acid content (such as MUFAs and linoleic acid). On the third experimental day, minor changes in the compositions of the digestive gland phospholipid fatty acid were noted, mainly in response to 100 μg/L cadmium (including an increase in arachidonic acid content); however, in triacylglycerols (under 100 μg/L cadmium), the level of saturated fatty acids decreased, and the unsaturation index increased (Fig. 4-Fig. 7).

3.2. Lipid peroxidation products

The content of the LPO products increased in contrast with that of the control in both the gills and digestive glands of *A. cygnea* in all cadmium-treated groups of mussels throughout the exposure period (Table 1, Table 2).

Gills

On the first experimental day, a significant increase in the CoD content of the gills of the mussels from all experimental aquariums was observed (Table 1). Unlike that in the digestive glands, the MDA content in the gills was lower, and the CoT and SchB distributions were equal. On the third experimental day, the content of the LPO products in the gills decreased slightly, except for mussels under 100 μg/L cadmium, which contained a higher level of MDA, CoT, and SchB (Table 1).

Digestive glands

On the first experimental day, an increase in the contents of CoD and MDA in the digestive glands was observed under 10 and 50 μg/L cadmium (Table 2). Under 100 μg/L cadmium, a slight increase in the contents of CoD and MDA was noted. The content of CoT increased slightly in all experimental groups of mussels. The accumulation of the end LPO product - Schiff bases - was significant under cadmium concentrations of 50 and 100 μg/L (Table 2). On the third experimental day, the distribution of CoD in the experimental groups of the mussels remained the same, but the differences became more pronounced (Table 2). In contrast, the accumulation of the secondary LPO products (MDA and CoT) and SchB were more pronounced in the mussels under 100 μg/L cadmium.

4. Discussion

4.1. Lipid peroxidation products changes under cadmium effect

The gills in bivalve mollusks are the primary organs exposed to environmental factors (Avery et al., 1998; Marigómez et al., 2002). They serve as the main site of metal accumulation in mussels, making gills more susceptible to the actions of toxicants (Chelomin et al., 1998; Marigómez et al., 2002). It was shown that modifications in various metabolic parameters in the gills of marine and freshwater mussels indicate their primary reaction to environmental effects (Avery et al., 1998; Fokina et al., 2013; Wadige et al., 2014). Cadmium is a highly toxic trace metal that initiates the accumulation of LPO products (Viarengo et al., 1990; Valko et al., 2005). Some of the primary LPO products are conjugated dienes (CoD) (Sevanian and Hochstein, 1985; Gutteridge and Halliwell, 1990). In the present study, we found a higher CoD content in the gills of *A. cygnea* compared

Table 1. Content of lipid peroxidation products in gills of freshwater mussels *A. cygnea*.

Cadmium, μg/L	Conjugated dienes, nM/g tissue	Malondialdehyde, nM/g tissue	Conjugated trienes, RU	Schiff bases, RU
24 h				
control	18.44 ± 1.85^{a}	4.07 ± 0.44^{a}	0.23 ± 0.01^{a}	0.02 ± 0.003^{a}
10	66.70 ± 9.86*^{a}	7.77 ± 0.37*^{a}	0.33 ± 0.02*^{b}	0.02 ± 0.002^{b}
50	74.49 ± 6.91*^{a}	10.54 ± 0.46*^{ab}	0.50 ± 0.01*^{a}	0.05 ± 0.003*^{a}
100	67.21 ± 9.70*^{a}	6.04 ± 0.35*^{b}	0.52 ± 0.02*^{ab}	0.13 ± 0.011*^{ab}
72 h				
control	14.14 ± 0.96^{a}	5.40 ± 0.54^{a}	0.32 ± 0.01^{a}	0.02 ± 0.003^{a}
10	30.81 ± 0.86*^{a}	9.35 ± 0.66*^{a}	0.46 ± 0.03*^{b}	0.03 ± 0.005*^{b}
50	22.56 ± 1.65*	8.51 ± 0.32*^{b}	0.64 ± 0.03*^{a}	0.08 ± 0.006*^{a}
100	23.81 ± 2.05*^{a}	15.69 ± 0.68*^{ab}	0.80 ± 0.02*^{ab}	0.22 ± 0.021*^{ab}

* – significant differences between control and experimental groups (Mann-Whitney test, $P < 0.05$);
$^{a\text{-}ab\text{-}b}$ – differences between control and experimental groups (Kruskal-Wallis test, $P < 0.05$);
RU – relative units

to that in the digestive glands. In addition, an increased level of the primary LPO products was observed in the gills of the mussels on the first experimental day. It is likely due to the accumulation of cadmium in the gills, thereby inducing oxidative stress. The CoD accumulation rates in the gills and digestive glands of the mussels were significantly lower on the third experimental day in comparison with the rates at the beginning of the experiment (r = -0.57 and r = -0.39, respectively). This indicates the progress of LPO processes and the prevalence of the propagation stage on the third day of the experimental cadmium treatment. At the same time, subsequent LPO products - malondialdehyde (MDA) and conjugated trienes (CoT) - accumulated in the gills (r = 0.32 and r = 0.43), as well as Shiff bases (SchB) − in the digestive glands (r = 0.41). Moreover, the accumulation of MDA, CoD (only in the gills), CoT and one of the end LPO products – SchB – had a dose-dependent effect in both the gills and digestive glands; an increase in these peroxidation products was observed under elevated cadmium dose effects (Table 1, Table 2). Perhaps the combined dose- and duration-effects are crucial for developing the oxidative stress and, consequently, accumulate LPO products in the gills and digestive glands of *A. cygnea*.

4.2. Lipid composition changes under cadmium effect

There were no significant changes in the total lipid composition of the *A. cygnea* gills, except for increased content of sterols on the first experimental day (significant only under 100 μg/L cadmium). A similar effect was observed in the digestive glands of *A. cygnea* under a one-day effect of 10 and 100 μg/L cadmium. In marine and freshwater mussels, the dominant sterol is cholesterol, which is necessary for the regulation of membrane permeability. It is known that the consequence of LPO activation is a disruption of membrane phospholipids and enhanced non-selective permeability of membranes (Oxidative stress..., 2011). The presence of cholesterol in cell membranes changes their susceptibility to peroxidation processes, likely by both intercepting some of the radicals and affecting the internal structure of the membrane through interaction with phospholipid fatty acids (Repetto et al., 2012). In the gills, there was a decrease in the sterol ester content, which probably replenishes the cholesterol reserves under a prolonged (three-day) cadmium effect. Previously, we showed a significant decrease in the cholesterol and phosphatidylcholine content in the digestive glands of the marine mussels, *Mytilus edulis*, on the first day of the cadmium effect, indicating destructive changes in the membranes (Fokina et al., 2013). Probably, in the freshwater mussels, *A. cygnea,* elevated cholesterol content maintains membrane integrity under the toxic effects of cadmium, except for three-day 100 μg/L cadmium effects. In this case, there was a significant decrease in phospholipids and their fractions. It is assumed that a significant accumulation of LPO products (such as CoD, MDA, CoT, and SchB) in the gills on the third day under 100 μg/L cadmium treatment, as well as a reduction in phospholipid content (PC, PE and LPC as predominant fractions and PI, PS and SM as minor fractions), indicates destructive changes in gill membranes. Along with an increase in the sterol content in the digestive glands, there was an increase in the contents of PC (on the first day) and PS (on the third day). The increased content of the dominant membrane phospholipid – PC – in the digestive glands caused by one-day 10 and 100 μg/L cadmium treatment presumably reflects a compensatory reaction in lipid metabolism on metal-induced oxidative stress. Significant increases in triacylglycerol (TAG) and phosphatidylserine (PS) content in the digestive glands of *A. cygnea* under cadmium effects can serve as a nonspecific biomarker reflecting the toxic effects of pollutants on bivalves. It is known that the accumulation of neutral lipids (including TAG) in the digestive glands of mussels is caused by an increase in the number of lysosomes and/or autophagosomes that supply autophagy processes (Moore et al., 2007; Koukouzika and Dimitriadis, 2008). Similar stress-inducible changes in TAG content were

Table 2. Content of lipid peroxidation products in digestive glands of freshwater mussels *A. cygnea*

Cadmium, μg/L	Conjugated dienes, nM/g tissue	Malondialdehyde, nM/g tissue	Conjugated trienes, RU	Schiff bases, RU
24 h				
control	24.95 ± 1.68 [a]	4.84 ± 0.37 [a]	0.15 ± 0.01 [a]	0.02 ± 0.002 [a]
10	68.54 ± 9.43*[a]	12.41 ± 0.72* [ab]	0.23 ± 0.01*	0.02 ± 0.003 [b]
50	59.31 ± 8.41*[a]	10.79 ± 0.81* [a]	0.28 ± 0.01* [a]	0.06 ± 0.005*[a]
100	46.16 ± 1.97*	7.29 ± 0.67* [b]	0.26 ± 0.02* [a]	0.16 ± 0.005*[ab]
72 h				
control	16.04 ± 1.10 [a]	5.35 ± 0.47 [a]	0.15 ± 0.01 [a]	0.02 ± 0.003 [a]
10	65.83 ± 2.89*[ab]	9.46 ± 0.71* [a]	0.24 ± 0.01* [a]	0.10 ± 0.012* [b]
50	20.41 ± 1.33*[b]	6.17 ± 0.62 [b]	0.22 ± 0.01* [b]	0.14 ± 0.008* [a]
100	34.72 ± 3.59*[a]	13.46 ± 0.78* [ab]	0.38 ± 0.02*[ab]	0.28 ± 0.021*[ab]

* – significant differences between control and experimental groups (Mann-Whitney test, $P < 0.05$);
[a-ab-b] – differences between control and experimental groups (Kruskal-Wallis test, $P < 0.05$);
RU – relative units.

observed in marine mussels under the impacts of pollutants (Koukouzika and Dimitriadis, 2008; Fokina et al., 2013). Additionally, the accumulation of PS in response to the toxic effects of cadmium and copper was noted in the marine mussels, *Mytilus edulis* (Fokina et al., 2013). Given the important role of PS in the activity regulation of membrane-bound enzymes (especially Na^+/K^+-ATPase), as well as TAG serving as a source of metabolic energy, we may use TAG and PS content as universal biomarkers whose changes reflect the toxic impact of pollutants for both marine and freshwater mollusks.

4.3. Fatty acid composition of freshwater mussels

The fatty acid composition of the gills and digestive glands of *A. cygnea* is influenced by the benthic habitat (Napolitano, 1999; Kelly and Scheibling, 2012), which contains freshwater organic matter derived from various autochthonous and allochthonous sources, including algae, vascular plants, and decaying plant and animal materials. The lipids of these organic materials contain long-chain saturated fatty acids and monounsaturated fatty acids (Napolitano, 1999). The predominant fatty acids of the phospholipids and triacylglycerols in the gills and digestive glands of *A. cygnea* were saturated fatty acids (33 – 41 % of the sum of fatty acids), especially palmitic 16:0 acid, stearic 18:0 acid and lignoceric 24:0 acid. Unsaturated fatty acids were dominated by monounsaturated fatty acids (27 – 32 % of sum of fatty acids), mainly 20:1 isomers representing 11-19 % of sum of fatty acids, as well as n-6 polyunsaturated fatty acids (18-21 % of sum of fatty acids), primarily due to linoleic 18:2n-6 and arachidonic 20:4n-6 acids (3.1-5.0 and 10-14 % sum of fatty acids, respectively). The content of n-3 PUFAs was significantly lower than that of n-6 PUFAs and constituted 10 – 15 % of the sum of fatty acids. Eicosapentaenoic 20:5n-3 and docosahexaenoic 22:6n-3 acids were 1.6 - 4.5 and 0.9 - 2.4 % of the sum of fatty acids, respectively. The enlarged content of 18:2n-6 and 20:4n-6 acids in the lipids of freshwater animals is described in detail in comparative studies of marine and freshwater organism fatty acid compositions (Napolitano, 1999). Changes in the fatty acid composition of *A. cygnea* under cadmium experimental effects reflect the features of the fatty acid composition in freshwater mussels. It is known that the predominant polyunsaturated fatty acids in the lipids of marine mussels (including *Mytilus edulis*) are n-3 PUFAs (mainly eicosapentaenoic 20:5n-3 and docosahexaenoic 22:6n-3 acids) (Fokina et al., 2013; Fokina et al., 2018). The fatty acid composition of *A. cygnea* was characterized by the dominance of n-6 PUFAs and monounsaturated 20:1 fatty acids. Therefore, the main target for cadmium-induced oxidation processes was polyunsaturated fatty acids with 3 or more double bonds, especially arachidonic 20:4n-6 acid (unlike 20:5n-3 and 22:6n-3 in marine mussels as it was described in Fokina et al. (2013) and Merad et al. (2017).

4.4. Fatty acid composition changes under cadmium effect

On the first experimental day of cadmium treatment, a significant decrease in the proportions of the phospholipids and triacylglycerol unsaturated fatty acids (mostly linoleic 18:2n-6 and arachidonic 20:4n-6 acids), as well as monounsaturated 20:1 acids, was noted in the gills of *A. cygnea* (Fig. 4-Fig. 7). At the same time, there was an increase in the proportion of saturated fatty acids and a decrease in the unsaturation index. Simultaneously, the increases in the contents of CoD, MDA and CoT are oxidation products of polyunsaturated fatty acids that contain 3 or more double bounds and indicate the activation of the oxidative and destructive processes in the gill membranes. It should be noted that on the third experimental day, the proportions of the unsaturated fatty acids, mainly n-6 PUFA, were restored both in the phospholipids and triacylglycerols. Probably, in the gills (organ of primary accumulation of metals) on the third experimental day, compensatory changes in the composition of the phospholipids and triacylglycerol unsaturated fatty acids through additional PUFA synthesis provide the restoration of unsaturation level of lipids under cadmium-induced oxidative stress.

In the composition of the digestive gland phospholipid fatty acids, on the first experimental day of the exposure to 50 μg/L of cadmium, modifications similar to those observed in *A. cygnea* gills on the third day of cadmium exposure (decrease in the proportions of saturated fatty acids and increase in unsaturation index) were observed. Most likely, there is a compensation of cadmium-induced oxidative stress through an increase in unsaturation of the lipids. At the same time, under 100 μg/L cadmium, the proportions of saturated fatty acids increased, and the unsaturation index decreased (these modifications were noted in the *A. cygnea* gills on the first day). It likely indicates the destructive oxidative processes in the digestive gland membranes caused by cadmium. Unlike phospholipid fatty acid composition, changes in the composition of triacylglycerol fatty acids were independent of cadmium concentration. On the first experimental day, there was an increase in the proportions of saturated fatty acids and a decrease in the 20:1 monounsaturated fatty acid content. On the third experimental day, there was an increase in the fatty acid unsaturation index (significant only for 100 μg/L cadmium).

5. Conclusions

Thus, the study of the lipid peroxidation products revealed the activation of cadmium-induced oxidative processes in the gills and digestive glands of *A. cygnea* under the experimental conditions. The different degrees of LPO product accumulation in the organs of the mussels reflected the intensity of the different stages of LPO and were also determined by the concentration and duration of the cadmium effect. Changes in the lipid composition of the *A. cygnea* gills and digestive glands were determined by the target organ, concentration and duration of cadmium exposure. In the fatty acid composition of the membrane lipids (phospholipids) of the gills, a significant decrease in the unsaturation level was observed on the first experimental day of the cadmium treatment. Together with a high level of LPO products, it indicated the activation of oxidative processes. In addition, the increased cholesterol content in the gills and digestive glands of *A. cygnea* on the first experimental day apparently decreased the non-selective ion permeability of the membranes. There was a restoration in the level of unsaturation of the fatty acids both in the phospholipids and

triacylglycerols in the gills of *A. cygnea* after prolonged cadmium exposure on the third day. Some lipid indices (in particular, phosphatidylserine and triacylglycerol content) that can be used as universal biomarkers of the toxic effects of cadmium were revealed. The increased content of these lipids in the organs of the mussels (mainly in digestive glands) caused by the effects of the cadmium ions in both marine and freshwater mussels was observed. However, the changes in the fatty acid composition of the mussels under the effects of cadmium were determined by the features in the fatty acid profiles of marine and freshwater habitants. For example, it has been shown that arachidonic 20:4n-6 acid serves as the main target for cadmium-induced oxidative processes in freshwater mussels (unlike EPA and DHA in marine ones). Thus, assessment of oxidative stress biomarkers (LPO products) and the main targets for oxidative processes (lipid and their fatty acid composition) allows the evaluation of the consequences of cadmium-induced oxidative stress on the membrane and storage lipids of mussels. Moreover, it makes it possible to identify protective biochemical mechanisms (including lipid composition) that provide the high resistance of mussels to environmental pollution.

Acknowledgements

We are deeply grateful to I.V. Sukhovskaya for help in setting up the experiment. This study was supported by federal funding for governmental-order project theme no. 0218-2019-0076 (no. AAAA-A17-117031710039-3) and the Russian Foundation for Basic Research (project no. 17-04-01431_a).

Compliance with ethical standards

The authors have no conflicts of interest to declare.

References

Arduini A., Peschechera A., Dottori S. et al. 1996. High performance liquid chromatography of long-chain acylcarnitine and phospholipids in fatty acid turnover studies. Journal of Lipid Research 37: 684-689.

Avery E.L., Dunstan R.H., Nell J.A. 1998. The use of lipid metabolic profiling to assess the biological impact of marine sewage pollution. Archives of Environmental Contamination and Toxicology 35: 229-235. DOI: 10.1007/s002449900371

Bird R.P., Draper H.H. 1984. Comparative studies on different methods of malondialdehyde determination. Methods in Enzymology 90: 105–110.

Chelomin V.P., Belcheva N.N., Zakhartsev M.V. 1998. Biochemical mechanisms of adaptation to cadmium and copper ions in the mussel *Mytilus trossulus*. Russian Journal of Marine Biology 24: 330-336.

Engelbrecht F.M., Mari F., Anderson J.T. 1974. Cholesterol determination in serum: a rapid direction method. South African Medical Journal 48: 250-256.

Fokina N.N., Ruokolainen T.R., Nemova N.N. 2018. The effect of intertidal habitat on seasonal lipid composition changes in blue mussels, *Mytilus edulis* L., from the White Sea. Polar Record 54: 133-151. DOI: 10.1017/S0032247418000293

Fokina N.N., Ruokolainen T.R., Nemova N.N. et al. 2013. Changes of blue mussels *Mytilus edulis* L. lipid composition under cadmium and copper toxic effect. Biological Trace Element Research 154: 217-225. DOI: 10.1007/s12011-013-9727-3Folch J., Lees M., Stanley J. 1957. A simple method for isolation and purification of total lipids from animal tissues. The Journal of Biological Chemistry 226: 497-509.

Gavrilov V.B., Gavrilova A.R., Mazhul L.M. 1987. Analysis of methods for the determination of lipid peroxidation products in blood serum by the test with thiobarbituric acid. Voprosy Meditsinskoy Khimii [Questions of Medical Chemistry] 1: 118–121. (In Russian)

Geret F., Serafim A., Barreira L. et al. 2002. Effect of cadmium on antioxidant enzyme activities and lipid peroxidation in the gills of the clam *Ruditapes decussatus*. Biomarkers 7: 242-256. DOI: 10.1080/13547500210125040

Gladyshev M.I., Anishchenko O.V., Sushchnik N.N. et al. 2012. Influence of anthropogenic pollution on content of essential polyunsaturated fatty acids in links of food chain of river ecosystem. Contemporary Problems of Ecology 5: 376-385. DOI: 10.1134/S1995425512040051

Gutteridge J.M., Halliwell B. 1990. The measurement and mechanism of lipid peroxidation in biological systems. Trends in Biochemical Sciences 15: 129-135. DOI: 10.1016/0968-0004(90)90206-Q

Hill T., Lewicki P. 2007. STATISTICS Methods and Applications. A comprehensive reference for science, industry, and data mining: StatSofr Inc.

Hyshiktuyev B.S., Hyshiktuyeva N.A., Ivanov V.N. 1996. Methods of measuring of lipid peroxidation products in exhaled air condensate and their clinical significance. Klinicheskaia Laboratornaia Diagnostika [Clinical Laboratory Diagnostics] 3: 13–15. (in Russian)

Kelly J.R., Scheibling R.E. 2012. Fatty acids as dietary tracers in benthic food webs. Marine Ecology Progress Series 446: 1-22. DOI: 10.3354/meps09559

Koukouzika N., Dimitriadis V.K. 2008. Aspects of the usefulness of five marine pollution biomarkers, with emphasis on MN and lipid content. Marine Pollution Bulletin 56: 941-949. DOI: 10.1016/j.marpolbul.2008.01.043

Manly R., George W.O. 1977. The occurrence of some heavy metals in populations of the freshwater mussel *Anodonta anatina* (L.) from the River Thames. Environmental Pollution 14: 139-154. DOI: 10.1016/0013-9327(77)90106-9

Marigómez I., Soto M., Cajaraville M.P. et al. 2002. Cellular and subcellular distribution of metals in molluscs. Microscopy Research and Technique 56: 358-392. DOI: 10.1002/jemt.10040

Méndez-Armenta M., Ríos C. 2007. Cadmium neurotoxicity. Environmental Toxicology and Pharmacology 23: 350-358. DOI: 10.1016/j.etap.2006.11.009

Merad I., Bellenger S., Hichami A. et al. 2017. Effect of cadmium exposure on essential omega-3 fatty acids in the edible bivalve *Donax trunculus*. Environmental Science and Pollution Research 25: 18242–18250. DOI: 10.1007/s11356-017-9031-4

Moore M.N., Viarengo A., Donkin P. et al. 2007. Autophagic and lysosomal reactions to stress in the hepatopancreas of blue mussels. Aquatic Toxicology 84: 80-91. DOI: 10.1016/j.aquatox.2007.06.007

Napolitano G.E. 1999. Fatty acids as trophic and chemical markers in freshwater ecosystems. In: Lipids in freshwater ecosystems. New York, pp. 21-44.

Ohkawa H., Ohishi N., Yagi K. 1979. Assay for lipid peroxides in animal tissues by thiobarbituric acid reaction. Analytical Biochemistry 95: 351-358. DOI: 10.1016/0003-2697(79)90738-3

Oxidative stress in aquatic ecosystems. 2011. In: Abele D., Vazquez-Medina J.P., Zenteno-Savin T. (Eds.). London: John Wiley & Sons.

Perceval O., Pinel-Alloul B., Méthot G. et al. 2002. Cadmium accumulation and metallothionein synthesis in freshwater bivalves (*Pyganodon grandis*): relative influence of the metal exposure gradient versus limnological variability. Environmental Pollution 118: 5-17. DOI: 10.1016/S0269-7491(01)00282-2

Perrat E., Couzinet-Mossion A., Tankoua O.F. et al. 2013. Variation of content of lipid classes, sterols and fatty acids in gonads and digestive glands of *Scrobicularia plana* in relation to environment pollution levels. Ecotoxicology and Environmental Safety 90: 112-120. DOI: 10.1016/j.ecoenv.2012.12.019

Ravera O. 1984. Cadmium in freshwater ecosystems. Experientia 40: 1-14. DOI: 10.1007/BF01959096

Regoli F., Nigro M., Orlando E. 1998. Lysosomal and antioxidant responses to metals in the Antarctic scallop *Adamussium colbecki*. Aquatic Toxicology 40: 375-392. DOI: 10.1016/S0166-445X(97)00059-3

Repetto M., Semprine J., Boveris A. 2012. Lipid peroxidation: chemical mechanism, biological implications and analytical determination. In: Catala A. (Ed.), Lipid peroxidation. Rijeka, pp. 3-31. DOI: 10.5772/45943

Sevanian A., Hochstein P. 1985. Mechanisms and consequences of lipid peroxidation in biological systems. Annual Review of Nutrition 5: 365-390.

Sidorov V.S., Lizenko E.I., Bolgova O.M. et al. 1972. Fish lipids. 1. Analysis technique. In: Potapova O.I., Smirnov Y.A. (Eds.), Lososevyye (Salmonidae) Karelii. Petrozavodsk, pp. 150-162. (in Russian).

Slukovskii Z.I., Ilmast N.V., Sukhovskaya I.V. et al. 2017. The geochemical specifics of modern sedimentation processes on the bottom of a small lake Lamba under technogenic impact. Trudy Karel'skogo Nauchnogo Tsentra Rossiyskoy Akademii Nauk [Transactions of Karelian Research Centre of Russian Academy of Science] 10: 45-63. DOI: 10.17076/lim618 (in Russian)

Suzuki R., Noguchi R., Ota T. et al. 2001. Cytotoxic effect of conjugated trienoic fatty acids on mouse tumor and human monocytic leukemia cells. Lipids 36: 477-482. DOI: 10.1007/s11745-001-0746-0

Traverso N., Menini S., Maineri E.P. et al. 2004. Malondialdehyde, a lipoperoxidation-derived aldehyde, can bring about secondary oxidative damage to proteins. The Journals of Gerontology Series A: Biological Sciences and Medical Sciences 59: 890-895. DOI: 10.1093/gerona/59.9.B890

Valko M.H.C.M., Morris H., Cronin M.T.D. 2005. Metals, toxicity and oxidative stress. Current Medicinal Chemistry 12: 1161-1208. DOI: 10.2174/0929867053764635

Viarengo A., Canesi L., Pertica M. et al. 1990. Heavy metal effects on lipid peroxidation in the tissues of *Mytilus galloprovincialis* lam. Comparative Biochemistry and Physiology Part C: Comparative Pharmacology 97: 37-42. DOI: 10.1016/0742-8413(90)90168-9

Wadige C.P.M., Maher W.A., Taylor A.M. et al. 2014. Exposure–dose–response relationships of the freshwater bivalve *Hyridella australis* to cadmium spiked sediments. Aquatic Toxicology 152: 361-371. DOI: 10.1016/j.aquatox.2014.04.016

Waller R.L., Recknagel R.O. 1977. Determination of lipid conjugated dienes with tetracyano-ethylene-14C: Significance for study of the pathology of lipid peroxidation. Lipids 12: 914-921. DOI: 10.1007/BF02533311

Xia L., Chen S., Dahms H.U. et al. 2016. Cadmium induced oxidative damage and apoptosis in the hepatopancreas of *Meretrix meretrix*. Ecotoxicology 25: 959-969. DOI: 10.1007/s10646-016-1653-7

Limnology and Freshwater Biology 2019 (5): 297-301 DOI:10.31951/2658-3518-2019-A-5-297

Original Article

ISSN 2658-3518
LIMNOLOGY FRESHWATER BIOLOGY
www.limnolfwbiol.com

Valve morphogenesis and silicon dynamics in the synchronized culture of *Ulnaria danica*

Bedoshvili Ye.D., Volokitina N.A., Marchenkov A.M.*

Limnological Institute, Siberian Branch of the Russian Academy of Sciences, Ulan-Batorskaya Str., 3, Irkutsk, 664033, Russia

ABSTRACT. Formation of diatom siliceous cell walls occurs inside the cells and depends on the availability of silicon from the environment. In the current work we have studied the valve morphogenesis of a freshwater pennate diatom *Ulnaria danica* in a laboratory culture synchronized by silica starvation and absence of light. Approximate timelines were established for the initiation of valve synthesis and formation of its major components. It was shown that the silicon surge uptake takes place, e.g. silicon concentration in the medium reduces during the first 30 minutes after the addition of silicon to a synchronized culture. During the formation of main valve elements, intracellular silicon pool is lower than it is after the end of synchronization, returning to the original level only 90 minutes after the addition of silica and beginning of the morphogenesis.

Keywords: diatoms, synchronized culture, morphogenesis, *Ulnaria danica*

1. Introduction

Diatom algae are unicellular autotrophic organisms that create species-specific siliceous structures at micro- and nanoscale. Mechanisms that regulate a process of silicon absorption from the environment and its transport to the silica deposition vesicle are related to the subsequent valve formation processes, but currently they are poorly understood. Diatom cell wall consists of two structures called valves, each connected to a system of ring-shaped girdle bands. All cell wall components synthesized sequentially inside the cell in a specialized organelle called silica deposition vesicle (SDV) (Reimann, 1964; Drum and Pankratz, 1964). Silicon is mostly available to diatoms as undissociated silicic acid (Martin-Jézéquel et al., 2000) which is imported to the cell by a SIT protein (Hildebrand et al., 1997; Hildebrand et al., 1998; Petrova et al., 2007; Sapriel et al., 2009). When silicic acid is abundant in the environment, diatom cells use it to build valves and girdle bands immediately after it is imported. Under the culturing conditions, though, the medium contains a limited amount of silicic acid. When cells are starved for silicon, they start "preparing" for a potential future silicon addition, and a small amount of currently available silicon forms an intracellular pool, which is probably stored in silica-containing inclusions (Grachev et al., 2017). After silicon is added to the environment, the cells respond by impulsively consuming silicic acid and immediately spending it on cell wall formation (Thamatrakoln and Hildebrand, 2008).

The majority of valve morphogenesis studies are performed on marine diatom species. Two most common model objects are *Thalassiosira pseudonana* (Thamatrakoln et al., 2012) and *Phaeodactylum tricornutum* (Armbrust et al., 2004), a centric and a pennate diatoms, both marine. Large-scale studies of a freshwater diatom frustule morphogenesis are being performed on the pennate species *Fragilaria radians* (Kütz.) D.M. Williams & Round for the last twenty years by Limnological Institute SB RAS (Grachev et al., 2002; Kaluzhnaya and Likhoshway, 2007; Safonova et al., 2007; Kharitonenko et al., 2015; etc.).

Diatoms are quiet diverse group of unicellular eukaryotes. Despite their common ability to synthesize silica exoskeletons by silicic acid extraction from water environment the phylogenetic diversities between different diatom groups are comparable with ones of humans and fishes. For this reason, to detect unknown participants of valve morphogenesis it is necessary to compare both species with a very different valve structure and more similar ones. For example, *Fragilaria radians* and *Ulnaria danica* (Kütz.) Compère & Bukhtiyarova are two closely related species. After a recent revision of genus *Synedra*, its species were reassigned to different genera: *S. acus* subsp. *radians* is considered synonymous to *Fragillaria radians* (Kütz.) D.M. Williams & Round (Williams and Round, 1987), and *S. ulna* subsp. *danica* is synonymous to *Ulnaria danica* (Kütz.) Compère & Bukhtiyarova (Bukhtiyarova and Compère, 2006). A comparison of the processes of valve morphogenesis and silicon uptake of such morphologically similar species has not been carried

*Corresponding author.
E-mail address: marchenkov.am@bk.ru (A.M. Marchenkov)

out previously.

The aim of this work was to establish the connection between cell wall morphogenesis and silicon dynamics (inside and outside the cell) in *Ulnaria danica*, as well as compare its valve morphogenesis stages to those of *Fragilaria radians*.

2. Materials and methods

The *Ulnaria danica* culture was grown in glass bottles with volume at 15 L during 16 days in DM medium for freshwater diatoms (Thompson et al., 1988) under natural illumination. Then cells were synchronized according to the protocol published earlier (Kharitonenko et al., 2015). Briefly, the cell biomass was concentrated on the polycarbonate filters with pore diameter 5 μm (Reatrack, Russia) and passed to DM medium without silicon. The cells were exposed during three days in the darkness at 16 ˚C in polycarbonate bottle with volume 16 L and then concentrated again. The part of these cells was used in the further experiment for SEM and silicon concentration determination. The main part of cell biomass were passed into the DM medium with silicon in the form of sodium metasilicate (Na_2SiO_3*$9H_2O$, 57 mg/L). After this five samples were taken after 30, 60, 90 and 120 minutes. The cells for determination of intracellular silicon pool were frozen with liquid nitrogen and then stored at -20 ˚C.

For further electron microscopy, the cell culture was concentrated by sequential centrifuging, washed in three changes of 6 % SDS for 30 minutes in a water bath (95 ˚C), washed five times in distilled water, placed in concentrated 68.4% nitric acid and incubated for 1 hour in a water bath (95 ˚C). After an hour, nitric acid was removed, and cells were washed thrice with ethanol, treated for 24 hours with 36 % hydrochloric acid and washed in water at least five times. Suspensions of cleaned valves were placed on SEM stubs, gold-coated in an SCD 004 sputter coater (Balzers) and examined on the Quanta 200 FEI Company (USA) scanning electron microscope. Valves were counted among 200 randomly encountered.

Silicon concentration in the medium and inside the cell was measured according to the published protocols (Guideline 52.24.433-95; Hervé et al., 2012). For determination intracellular silicon pool the frozen cells were resuspended in 1 ml of distilled water, incubated at 95 ˚C for 10 min, cooled and concentrated by centrifugation (1450 g) with centrifuge Allegra X-12R, Beckman Coulter (USA). The intracellular silicon in samples of supernatant as well as samples of the medium DM was measured using the silicomolybdate assay (Guideline 52.24.433-95) with standard sample of silicon solution (EKO-analitika, Russia) in a range of 0 to 12 mg/L. All measurements were taken in triplicate.

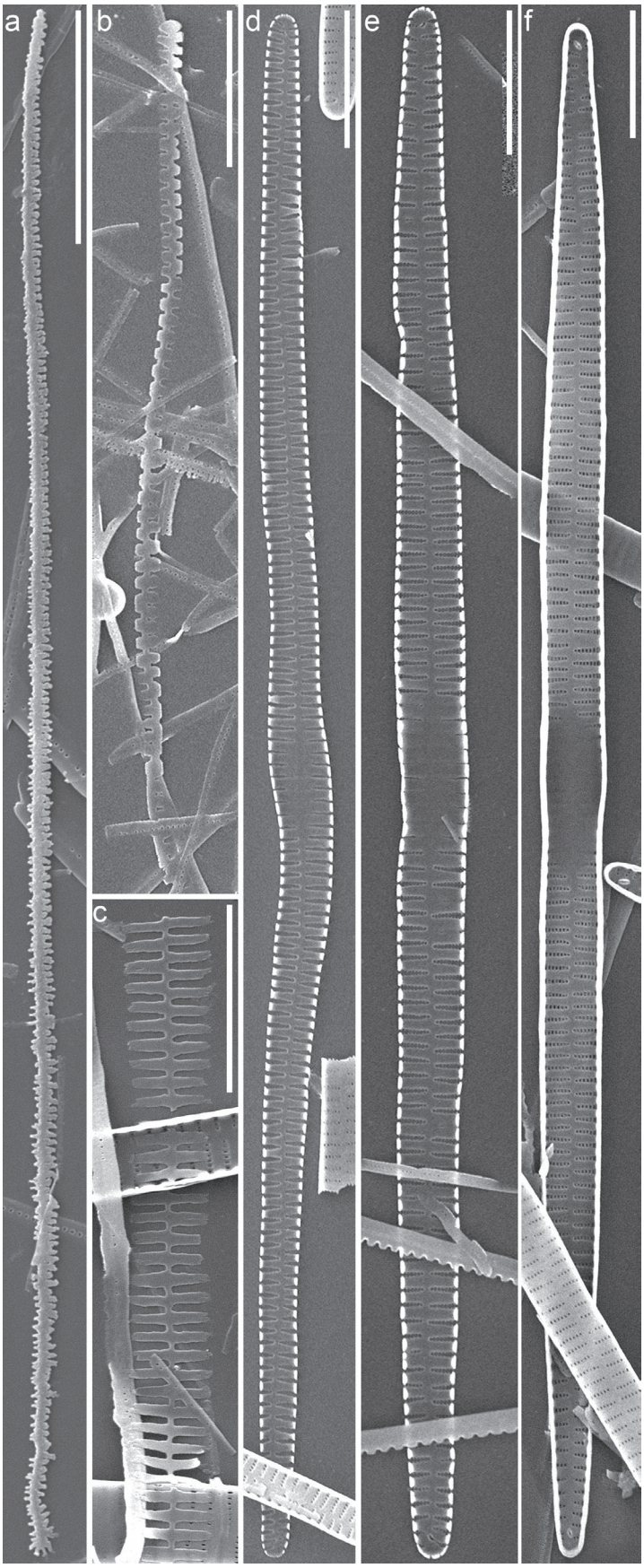

Fig. 1. The sequence of morphogenesis stages in *U. danica* (SEM). a — stage I, thread-like filament; b — stage II, virga formation; c — stage III, virga growth; d — formation of valve mantle; e — vimin formation; f — mature valve. The scale is 10 μm.

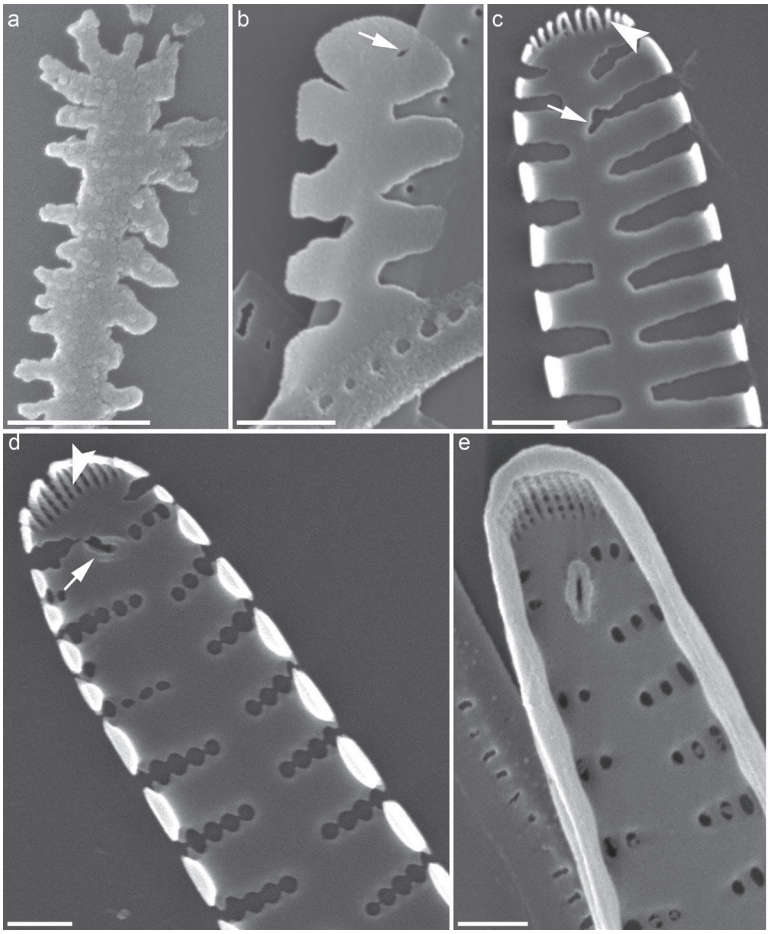

Fig. 2. The apex of *U. danica* valves at various morphogenesis stages. a — stage I; b — stage II; c — stage IV; d — stage V; e — mature valve. White arrows point to rimoportula, short ones point to apical pore area. The scale is 1 μm.

3. Results

Valves of a synchronized culture taken during 120 minutes after silicon addition were studied with SEM. Valve morphogenesis stages were identified by markers described for a related species *F. radians* (Kaluzhnaya and Likhoshway, 2007; Kharitonenko et al., 2015). The earliest stage that we have managed to register (**stage I**) is a sternum, long siliceous filament (Fig. 1a) with forming first-order branchings (virgae) that later merge and form mature virgae. At this stage the position of future rimoportula is yet unmarked (Fig. 2a) and the entire structure is rigid; unlike later stages, when valve can even bend in half, sternum always appeared straight.

The first signs of rimoportula appear on **stage II** (Fig. 1b, Fig. 2b) when virgae have already formed and are growing (**stage III**, Fig. 1c). Axial pore area starts developing from separate thin filaments at **stage IV**; by this time, valve mantle has started forming (Fig. 1d, Fig. 2c). Creation of second-order branchings (viminae) and axial pore area happens during **stage V** (Fig. 1e, Fig. 2d). Growth of velums on areolae apparently continues even after valve mantle is finished and valves appear to be fully formed (Fig. 1f, Fig. 2e).

Valves on different stages were found in all SEM preparations. However, in the sample taken 120 minutes after silica addition, all valves were on morphogenesis stages IV-V. The presence of the valves on different morphogenesis stages is shown in Table 1.

Measurements of silicon concentration in the medium have shown that it drops to less than half of the original level during 30 minutes after finishing three days of synchronization and introducing silicon to diatom culture (Fig. 3). For the next 2 hours the silicon concentration was either decreasing insignificantly or not decreasing at all. Silicon concentration in the intracellular silicon pool of synchronized culture (Fig. 4) was also decreasing during the first 60 minutes and returning to the original level after 90 minutes. The measured silicon concentration in the medium was above 57 mg/L, ranging from 62 mg/L to 83 mg/L. We suspect that this is caused by the DM preparation protocol, which involves using sodium metasilicate to reach the required pH.

4. Discussion

The stages of *U. danica* morphogenesis are similar to those in a previously described related species *F. radians* (Kharitonenko et al., 2015), although the earlier stages of valve forms happen quicker for *U. danica* than for *F. radians*, despite its larger size. Most of the primary valve morphogenesis (horizontal differentiation—Schmid and Volcani, 1983) took place during the first two hours after the end of synchronization. The order in which various morphological structures have

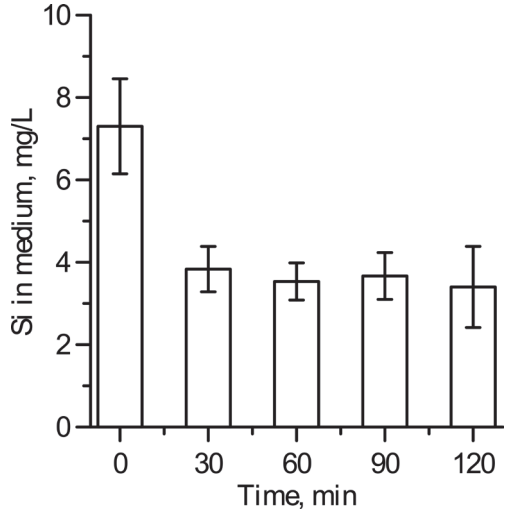

Fig. 3. The dynamics of silicon concentration in the medium.

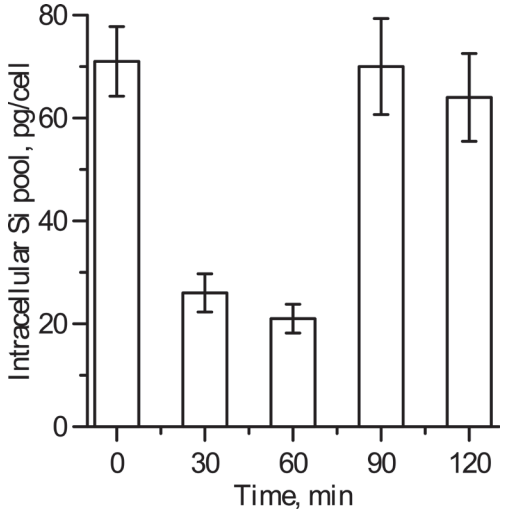

Fig. 4. The dynamics of silicon concentration in the cells.

appeared is the same as in *F. radians*; silica deposition itself first happens horizontally (like in other species — Schmid and Volcani, 1983), then the valve starts vertical differentiation and getting thicker.

It is interesting that forming sternum seems to have no flexibility, unlike valves on the later stages of development. This fact can demonstrate the variance in the state of silicic acid or general chemical composition of SDV contents between earlier and later morphogenesis stages. It is visible that at earlier stages virgae are more numerous and narrow; they are likely to merge at later stages similarly to *F. radians* (Kaluzhnaya and Likhoshway, 2007), but scanning electron microscopy cannot visualize this process in *U. danica*. Our data also show that even if rimoportula does indeed start forming at the earliest morphogenesis stages, it is not detectable at the sternum stage. The loop that later becomes rimoportula (Kaluzhnaya and Likhoshway, 2007, Fig. 26) doesn't appear until at least Stage II, during virga formation. Thus, the details described in this work extend the previously available information about valve morphogenesis in pennate diatoms (Cox and Kennaway, 2004).

It is known that assimilation of silicon by diatoms occurs according to Michaelis–Menten kinetics, and that silicon-starved cultures tend to quickly consume silicon from the environment when it becomes available (Conway and Harrison, 1977). The chemical analysis of silicon concentration has shown that it is consumed immediately, but for the first 60 minutes (during which the valve is built) its concentration inside the cell does not increase. *T. pseudonana* has slightly different kinetics of silicon use under similar conditions (Thamatrakoln and Hildebrand, 2008). Unlike *U. danica, T. pseudonana* does not store a significant amount of silicon during starvation, but does increase the intracellular silicon concentration after the cells are placed into a silicon-rich medium. The species we have studied, on the other hand, can accumulate silicon during starvation or keep its level constantly low; during silicon starvation, morphogenesis does not start, because otherwise the cell may not have enough material to finish the valve, which would probably be lethal. The intracellular silicon levels drop at the earlier stages of morphogenesis, when silica is actively deposited to the forming valve. Later, though, silica deposition speed decreases and intracellular silicon pool replenishes (this happens 90 minutes after providing silicon to synchronized cultures), because at later stages silica deposits slower and therefore is not consumed as quickly. That is why there is no significant silica concentration decrease in medium after the initial surge uptake (Fig. 3). The difference in silicon acquisition in spending between *T. pseudonana* and *U. danica* can be caused by the scale valve morphogenesis, since valve thickness and division time is several times higher in the latter. *T. pseudonana*,

Table. 1. The distribution of valves on different morphogenesis stages along sampling times.

	Time, min				
Stages of morphogenesis	0	30	60	90	120
I, Fig. 1a, Fig. 2a	-	+	-	-	-
II, Fig. 1b, Fig. 2b	-	+	+	-	-
III, Fig. 1c	-	+	+	+	-
IV, Fig. 1d, Fig. 2c	Sporadically	Sporadically	+	+	+
V, Fig. 1e, Fig. 2d	Sporadically	Sporadically	+	+	+

which has smaller cells and less thick walls, can afford to spend silicon on building valve and girdle bands as it is being absorbed from medium. The creation of intracellular silicon pool or maintenance of certain silicon level during its shortage in the environment has been documented in other diatoms (Azam, 1974; Sullivan, 1976; 1977).

Thus, in *U. danica* silicon accumulation is linked to the valve morphogenesis. This species can accumulate silicon inside the cell, although not during horizontal valve differentiation (at that time all incoming silicon is immediately consumed); but when there is no active silica deposition, its intracellular level remains constant.

Acknowledgments

The reported study was funded by RFBR according to the research project № 18-34-00438. The work was carried out in the Collective Instrumental Center 'Ultramicroanalysis' at the Limnological Institute of the Siberian Branch of RAS.

References

Armbrust E.V., Berges J.A., Bowler C. et al. 2004. The genome of the diatom *Thalassiosira pseudonana*: Ecology, evolution, and metabolism. Science 306: 1-33. DOI: 10.1126/science.1101156

Azam F. 1974. Silicic acid uptake in diatoms studied with [^{68}Ge] germanic acid as a tracer. Planta 121: 205-212. DOI: 10.1007/BF00389321

Bukhtiyarova L.N., Compère P. 2006. New taxonomical combinations in some genera of Bacillariophyta. Algology 16: 280-283.

Conway H.L., Harrison P.J. 1977. Marine diatoms grown in chemostats under silicate or ammonium limitations IV. Transient response of *Chaetoceros debilis*, *Skeletonema costatum*, and *Thalassiosira gravida* to a single addition of the limiting nutrient. Marine Biology 43: 33-43. DOI: 10.1007/BF00392568

Cox E., Kennaway G. 2004. Studies of valve morphogenesis in pennate diatoms: investigating aspects of cell biology in a systematic context. In: 17th International Diatom Symposium, pp. 35-48.

Drum R.W., Pankratz S. 1964. Pyrenoids, raphes, and other fine structure in diatoms. American Journal of Botany 51: 401-418. DOI: 10.2307/2439832

Grachev M.A., Denikina N.N., Belikov S.I. et al. 2002. Elements of the active center of silicon transporters in diatoms. Molecular Biology 36: 534-536. DOI: 10.1023/A:1019860628910

Grachev M.A., Bedoshvili Y.D., Gerasimov E.Y. et al. 2017. Silica-containing inclusions in the cytoplasm of diatom *Synedra acus*. Doklady Biochemistry and Biophysics 472: 44-48. DOI: 10.1134/S1607672917010124

Guideline 52.24.433-95. 1995. Guidelines for the determination of silicon in natural and treated wastewater. Rostov-on-Don, 8. (In Russian)

Hervé V., Derr J., Douady S. et al. 2012. Multiparametric analyses reveal the pH-dependence of silicon biomineralization in diatoms. PLoS One 7. DOI: 10.1371/journal.pone.0046722

Hildebrand M., Volcani B.E., Gassmann W. et al. 1997. A gene family of silicon transporters. Nature 385: 688-689. DOI: 10.1038/385688b0

Hildebrand M., Dahlin K., Volcani B.E. 1998. Characterization of a silicon transporter gene family in *Cylindrotheca fusiformis*: sequences, expression analysis, and identification of homologs in other diatoms. Molecular Genetics and Genomics 260: 480-486. DOI: 10.1007/s004380050920

Kaluzhnaya Ol.V., Likhoshway Ye.V. 2007. Valve morphogenesis in an araphid diatom *Synedra acus* subsp. *radians*. Diatom Research 22: 81-87. DOI: 10.1080/0269249X.2007.9705696

Kharitonenko K., Bedoshvili Ye., Likhoshway Ye. 2015. Changes in the micro- and nanostructure of siliceous frustule valves in the diatom *Synedra acus* under the effect of colchicine treatment at different stages of the cell cycle. Journal of Structural Biology 190: 73-80. DOI: 10.1016/j.jsb.2014.12.004

Martin-Jézéquel V., Hildebrand M., Brzezinski M.A. 2000. Silicon metabolism in diatoms: implication for growth. Journal of Phycology 36: 821-840. DOI: 10.1046/j.1529-8817.2000.00019.x

Petrova D.P., Bedoshvili Y.D., Shelukhina I.V. et al. 2007. Detection of the silicic acid transport protein in the freshwater diatom *Synedra acus* by immunoblotting and immunoelectron microscopy. Doklady Biochemistry and Biophysics 417: 295-298. DOI: 10.1134/S1607672907060014

Reimann B.E.F. 1964. Deposition of silica inside a diatom cell. Experimental Cell Research 34: 605-608. DOI: 10.1016/0014-4827(64)90248-4

Safonova T.A., Annenkov V.V., Chebykin E.P. et al. 2007. Aberration of morphogenesis of siliceous frustule elements of the diatom *Synedra acus* in the presence of germanic acid. Biochemistry (Moscow) 72: 1261-1269. DOI: 10.1134/s0006297907110132

Sapriel G., Quinet M., Heijde M. et al. 2009. Genome-wide transcriptome analyses of silicon metabolism in *Phaeodactylum tricornutum* reveal the multilevel regulation of silicic acid transporters. PLoS One 4. DOI: 10.1371/journal.pone.0007458

Schmid A.-M., Volcani B. 1983. Wall morphogenesis in *Coscinodiscus wailesii*. I. Valve morphology and development of its architecture. Journal of Phycology 19: 387-402. DOI: 10.1146/annurev-physiol-012110-142145

Sullivan C.W. 1976. Diatom mineralization of silicic-acid. I. $Si(OH)_4$ transport characteristics in *Navicula pelliculosa*. Journal of Phycology 12: 390-396. DOI: 10.1111/j.1529-8817.1976.tb02862.x

Sullivan C.W. 1977. Diatom mineralization of silicic acid. II. Regulation of $Si(OH)_4$ transport rates during the cell cycle of *Navicula pelliculosa*. Journal of Phycology 13: 86-91. DOI: 10.1111/j.1529-8817.1977.tb02892.x

Thamatrakoln K., Hildebrand M. 2008. Silicon uptake in diatoms revisited: A model for saturable and nonsaturable uptake kinetics and the role of silicon transporters. Plant Physiology 146: 1397-1407. DOI: 10.1104/pp.107.107094

Thamatrakoln K., Korenovska O., Niheu A.K. et al. 2012. Whole-genome expression analysis reveals a role for death-related genes in stress acclimation of the diatom *Thalassiosira pseudonana*. Environmental Microbiology 14: 67-81. DOI: 10.1111/j.1462-2920.2011.02468.x

Thompson A.S., Rhodes J.C., Pettman I. 1988. Culture collection of algae and protozoa: catalogue of strains. Kendal: Natural Environmental Research Council Press.

Williams D.M., Round F.E. 1987. Revision of the genus *Fragilaria*. Diatom Research 2: 267-288. DOI: 10.1080/0269249X.1987.9705004

Limnology and Freshwater Biology 2019 (5): 302-307 DOI:10.31951/2658-3518-2019-A-5-302

Original Article

ISSN 2658-3518
LIMNOLOGY FRESHWATER BIOLOGY
www.limnolfwbiol.com

Fluorescent dyes for the study of siliceous sponges

Danilovtseva E.N., Palshin V.A., Zelinskiy S.N., Annenkov V.V.*

Limnological Institute, Siberian Branch of the Russian Academy of Sciences, Ulan-Batorskaya Str., 3, Irkutsk, 664033, Russia

ABSTRACT. New fluorescent dyes containing coumarine and rhodamine groups were applied as vital dyes capable of staining growing siliceous spicules of Baikal sponge *Lubomirskia baicalensis* (Pallas, 1773). Cultivation of the sponge primmorphs in the presence of fluorescent dyes allows the use of confocal microscopy to study the morphology of the spicules and, in the case of two-color staining, to draw some conclusions about the growth rate of the spicules. 5-6.5 months were estimated to be the time required for the full formation of the spicules.

Keywords: siliceous sponge, fluorescent dye, vital staining, confocal microscopy, spicules

1. Introduction

Sponges are the oldest invertebrates, and they play an important role in aquatic ecosystems. Sponge skeleton consists of composite needle-like spicules based on silica or calcium carbonate. Spicules are linked by organic material (Fig. 1), forming three-dimensional structures filled with sponge cells and numerous symbionts: zoochlorellas, bacteria, viruses, dinoflagellates, diatoms, and fungi (Taylor et al., 2007). These symbionts are an inexhaustible source of biologically active compounds (Blunt et al., 2018; Carroll et al., 2019; El-Demerdash et al., 2019; Khalifa et al., 2019). Spicules of siliceous sponges are considered as prospective biogenic constructions for optic applications and a source of ideas of bioinspired materials (Zhang et al., 2016; Mcheik et al., 2018). Sponges are motionless organisms that filter out a huge amount of water through their bodies and are thus highly susceptible to the influence of harmful environmental factors. A disease of Baikal sponges (Denikina et al., 2016; Khanaev et al., 2018; Zvereva et al., 2019) is the striking manifestation of crisis phenomena in the Baikal coastal zone.

Experiments with sponges or with sponge cultures (primmorphs, (Wilson, 1907; Custodio et al., 1998)) are important for environmental and biotechnological investigations. The proper formation of the sponge spicules is important evidence of the organism's viability. Counting the new spicules during an experiment is a difficult and unobvious task, as it is impossible to distinguish between old and new spicules. Another intriguing question in the sponge physiology is what the growth rate of the spicules is. The spicule growth continues for days, and there are no harmless methods for observing individual spicule. Recently, we proposed to apply vital fluorescent dye NBD-N2 (green fluorescence, Fig. 1) for staining the growing siliceous spicules (Annenkov et al., 2014). This dye is accumulated in bio-silica such as sponge spicules and frustules of diatom algae which are obtained from cultivation in the presence of the dye.

This work is aimed at the application of other vital dyes (Fig. 2): Q-N2 (blue fluorescence) and Rhod-N3 (red fluorescence) for staining siliceous spicules of Baikal endemic sponge *Lubomirskia baicalensis* (Pallas, 1773). Q-N2 was previously studied in staining diatom frustules, and we found a change of blue fluorescence in solution to cyan emission in siliceous materials. The availability of several fluorescent dyes allowed us to interchange dyes during sponge cultivation and estimate the growth rate of the spicules.

2. Materials and methods

2.1. Chemical reagents

Bottled Baikal water was used for primmorph cultivation. Fluorescent dyes NBD-N2 and Q-N2 were obtained according to Annenkov et al., 2010; 2019. Rhod-N3H (Annenkov et al., 2016a) was synthesized (Fig. 3) following the approach reported in (Kwon et al., 2005). Briefly, rhodamine B was converted to the chloroanhydride and further reacted with N,N-bis[3-(methyamino)propyl]methylaamine (N3) to give the target Rhod-N3. The product was purified on a flash chromatography column packed with C18-reversed phase silica gel ($H_2O/CH_3CN/HCOOH = 63.2/36.7/0$, yield 18%). Other chemicals were purchased from Merck, Fisher or Acros Chemicals and used without

*Corresponding author.
E-mail address: annenkov@lin.irk.ru, annenkov@yahoo.com (V.V.Annenkov)

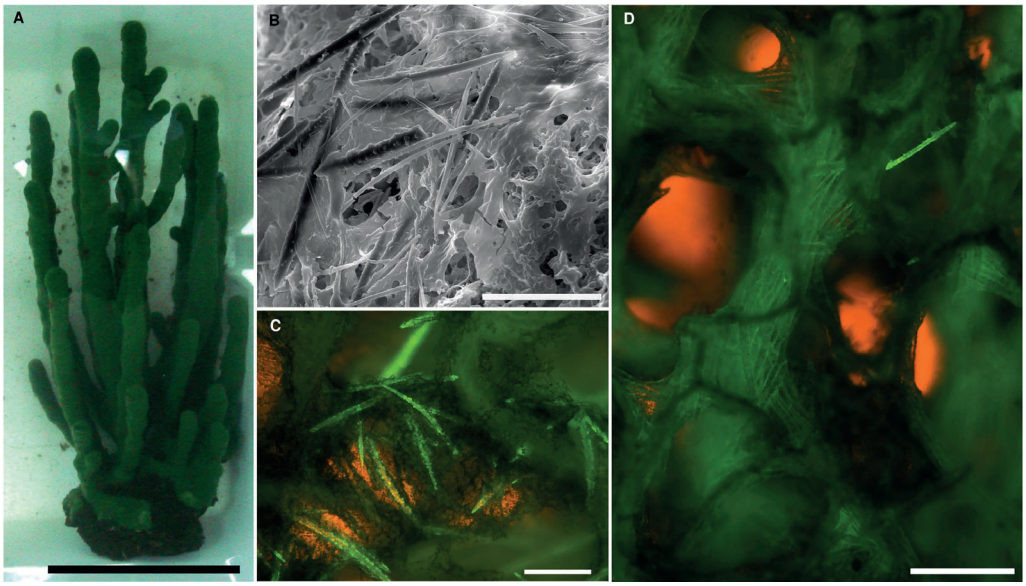

Fig. 1. Baikal sponge *L. baicalensis* collected for primmorph preparation (A); scanning electron microscopy (B) and combined light and fluorescent microscopy (C and D) images of the sponge spicules associated with organic material. Bright green spicules (C and D) are stained with NBD-N2 by the sponge cultivation in the presence of the dye during one month. Excitation was at 470 nm, and emission was observed above 515 nm. Scale bar represents 5 cm (A), 100 μm (B and C) and 200 μm (D).

further treatment.

2.2. Sponge samples and cultivation of primmorphs

Experiments with sponge samples and primmorphs were performed according to Annenkov et al., 2014; Annenkov and Danilovtseva, 2016b. Samples of *L. baicalensis* were collected near the village Bolshie Koty, in the southwestern part of Lake Baikal, from 10 m depth. Primmorphs were obtained similar to Custodio et al., 1998. Briefly, sponge samples were cut under Baikal water (3 °C) into ≈1-2 mm particles. The particles and water were transferred into 50 mL conical plastic tubes (sponge to water ratio ≈ 1: 20) and gently shaken for 15 min with a rotatory shaker. Then, the suspension was filtered through a 100 μm nylon net. The cells obtained were harvested by sedimentation (1 h, 3 °C) and washed again with Baikal water. The cell suspension was placed into 400 ml plastic containers with 200 ml of Baikal water containing 0.002 % of ampicillin. The containers were kept in the same conditions as sponge samples under cultivation. Every day during two weeks, 75% of the water was replaced by fresh water containing the antibiotic. After two weeks, the primmorphs obtained (1 mm and more in diameter) were moved to the new containers with water and antibiotic and 75% change of the water was performed weekly. At the same time, fluorescent dyes were added to the cultivation medium in 0.5 μM concentration. Experiments on the weekly change of the dyes were performed with triple washing of the primmorphs with the culture medium.

2.3. Study of Rhod-N3 toxicity

Experiments aimed at determination of the toxicity of Rhod-N3 towards diatoms were performed similar to (Annenkov et al., 2010). The synchronized culture of *Ulnaria ferefusiformis* (M.Kulikovskiy & H.Lange-Bertalot, 2016) was diluted with DM medium to a final concentration of 1000-3000 cell/mL and 90 μL of the suspension was added into every well of 96-well microcultivation flat bottom plate. Then, 10 μL of an appropriate solution of Rhod-N3 in the DM medium was added to every well. Experiments with each concentration of Rhod-N3 were repeated 5-6 times. The cultivation was performed at 18°C. A luminescent lamp was switched on and off at 12 h intervals and the light intensity at "daytime" was 16 μmoles/m^{-2}·sec^{-1}. The growth of the cells was observed during 7 days.

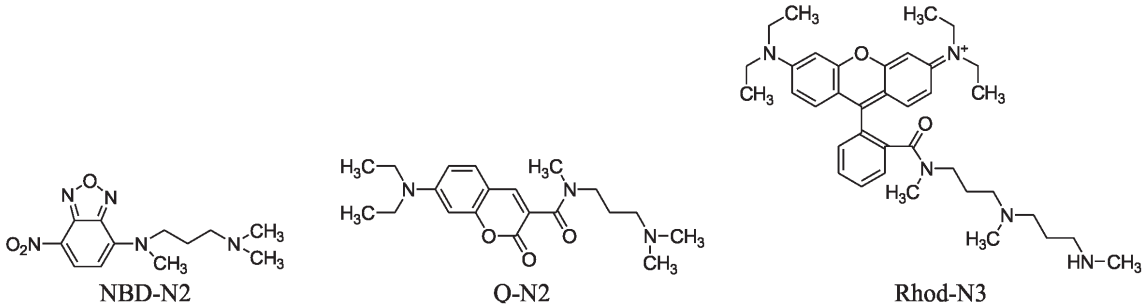

Fig. 2. Structures of the fluorescent dyes.

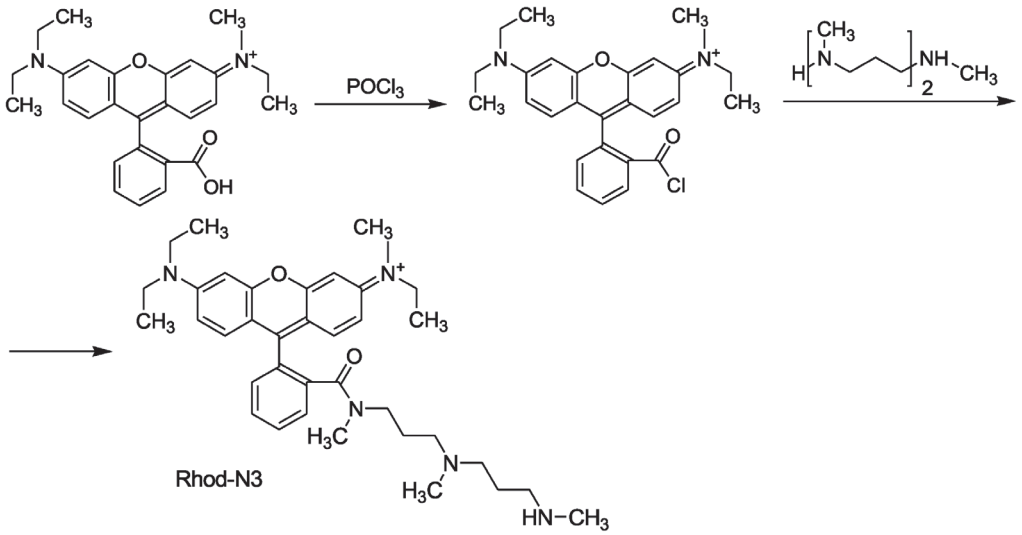

Fig. 3. Scheme of Rhod-N3 synthesis.

2.4. Instrumentation

UV–Vis absorption measurements were carried out using a Perkin Elmer Lambda 950 spectrophotometer. Photoluminescence spectra were recorded at 25 °C using a Perkin-Elmer LS-55 instrument. For absorption and fluorescence measurements the path length of the quartz cuvette was 1 cm.

Fluorescent microscopy was performed using an inverted microscope Motic AE-31T with an HBO 103 W/2 OSRAM mercury lamp. Excitation was at 470 nm, and emission above 515 nm was observed. Confocal images were obtained using a Zeiss LSM710 microscope with the following parameters: excitation 405, 488 or 561 nm; detector slit 410-585, 501-572 or 566-620 nm for Q-N2, NBD-N2 and Rhod-N3 dyes respectively with a ×63 oil immersion objective. For double color Q-N2 – NBD-N2 images: excitation 405 and 488 nm, detector slit 409-491 and 519-620 nm, respectively. For double color QN_2 – Rhod-N3 images: excitation 405 and 561 nm, detector slit 410-523 and 566-620 nm respectively.

3. Results and discussion

Absorption and fluorescence of new dye Rhod-N3 do not depend on pH in the 5.5-9.18 interval (Fig. 4). Fig. 5. Summarizes the fluorescent properties of NBD-N2, Q-N2, and Rhod-N3 dyes are summarized. NBD-N2 and Q-N2 do not have a significant effect on the growth of diatom algae in the 1 μm concentration (Annenkov et al., 2010; 2019), and 0.5 μm Rhod-N3 slightly depresses the diatom culture (Fig. 6).

Primmorphs of the Baikal sponge *Lubomirskia baicalensis* were cultivated in the presence of 0.5 μM Q-N2 and Rhod-N3 giving rise to fluorescent tagged spicules (Fig. 7). The formation of fluorescent vesicles in silicifying sponge cells (sclerocytes) was observed on the first day after adding the dye to the culture medium (Fig. 8). 350-450 nm stained layer was found in spicules after three days of cultivation, and a week growth in the presence of fluorescent dye resulted in a 550-650 nm stained layer.

Cultivation of the primmorphs with the addition of two dyes that were changed every week enabled to obtain layer-by-layer stained spicules which were studied with confocal microscopy. The parameters for confocal microscopy of the bicolored spicules were chosen from the fluorescent spectra of siliceous diatom frustules stained with the corresponding dyes (Fig. 9, Fig. 10). The confocal images were recorded using alternately two excitation lasers and two detector slits which corresponded to almost separate emission from

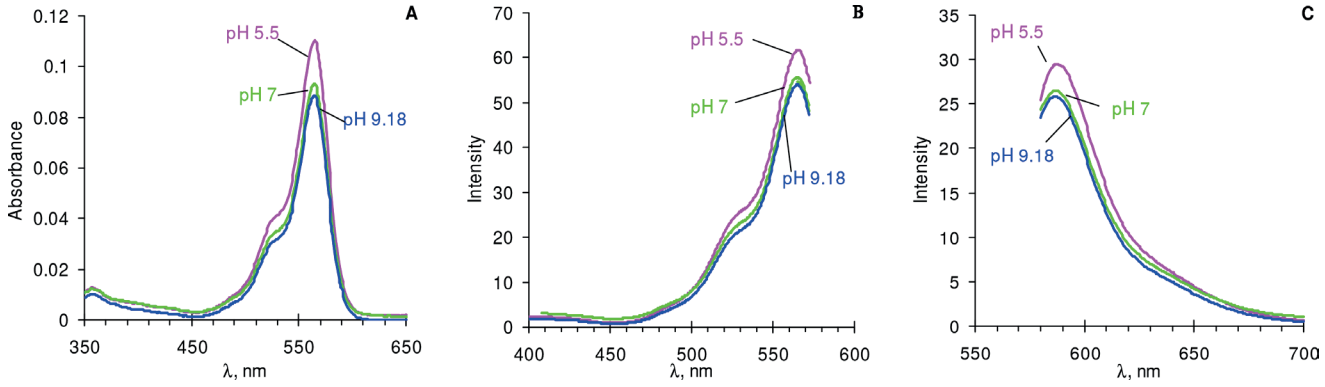

Fig. 4. The absorption (A), excitation (B) and emission (C) spectra of Rhod-N3 dye in aqueous solutions at pH 5.5, 7 and 9.18. The concentration of Rhod-N3 is 2.08 μM. Excitation spectra were recorded for emission at 587 nm, and 565 nm excitation was applied for emission spectra.

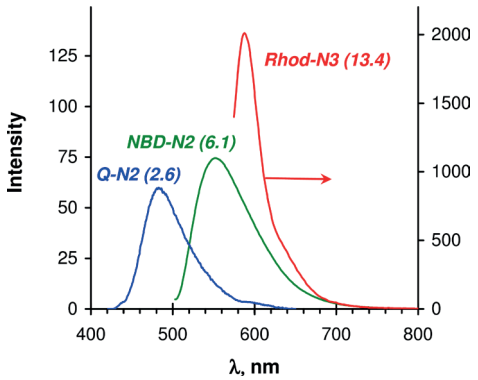

Fig. 5. Emission spectra and quantum yields (Q, %, in brackets) of NBD-N2, Q-N2 and Rhod-N3 dyes at pH 7. Solution concentration and excitation wavelength are 1, 1.5 and 1 μM, 490, 411 and 565 nm, respectively.

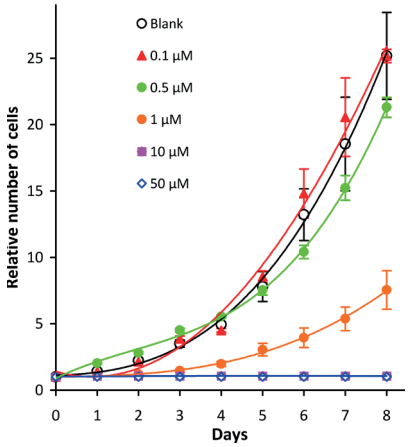

Fig. 6. Growth curves of *U. ferefusiformis* in the presence of Rhod-N3 dye. The concentration of the dye is presented on the chart.

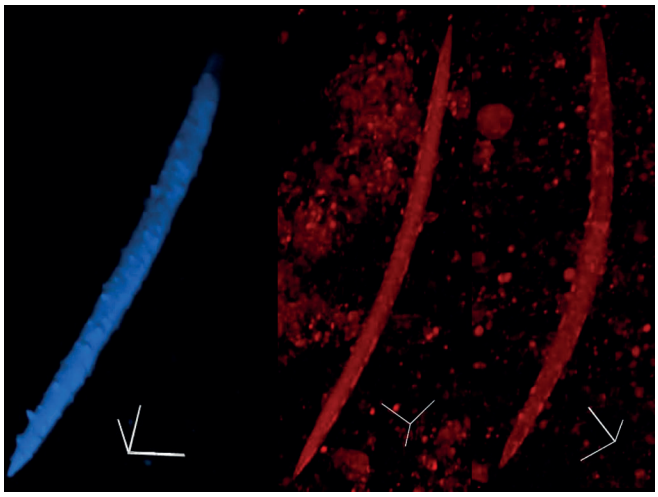

Fig. 7. 3D confocal images of *L. baicalensis* spicules obtained from primmorphs cultivated in the presence of Q-N2 (blue) and Rhod-N3 (red) dyes. Scale bar represents 10 μm.

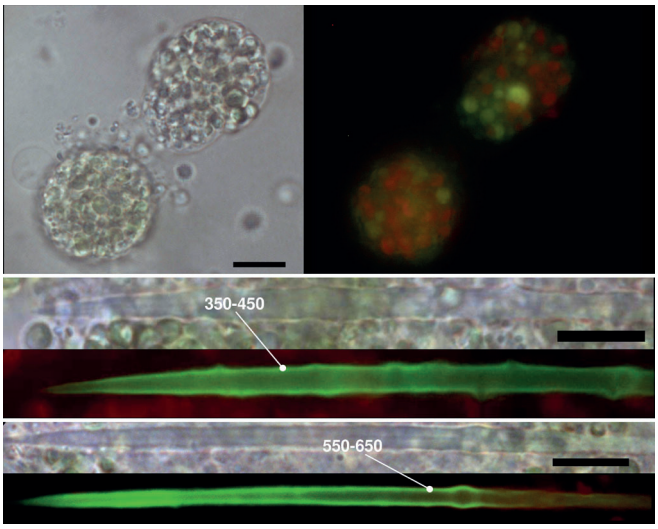

Fig. 8. Fluorescent images of cells in *L. baicalensis* primmorphs after one-day growth in the presence of 0.5 μM NBD-N2 (top) and spicules obtained on third (middle) and seventh (bottom) days after adding the dye to culture medium. Excitation was at 470 nm, and emission was observed above 515 nm. Scale bar corresponds to 10 μm.

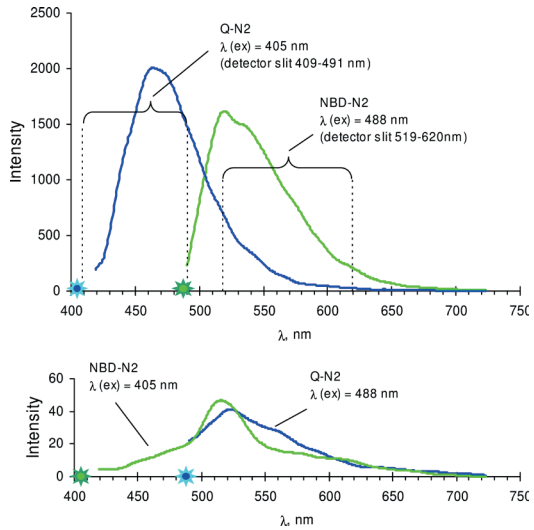

Fig. 9. Determination of excitation wavelength and detector slit for simultaneous observation of objects stained with Q-N2 and NBD-N2 dyes. *U. ferefusiformis* frustules stained by cultivation in the presence of these dyes were applied.

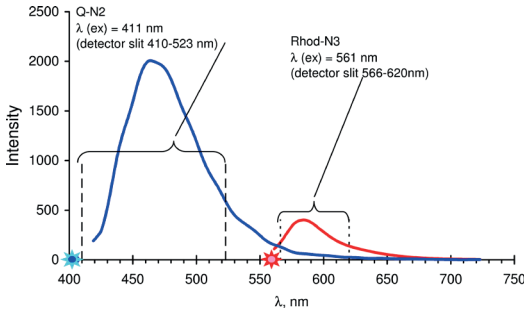

Fig. 10. Determination of excitation wavelength and detector slit for simultaneous observation of objects stained with Q-N2 and Rhod-N3 dyes. *U. ferefusiformis* frustules stained by cultivation in the presence of these dyes were applied. Q-N2 and Rhod-N3 do not show noticeable fluorescence at 561 and 411 nm excitation, respectively.

the dyes.

Images from the confocal microscopy (Fig. 11) allow estimating the thickness of the alternate silica layers that formed during one week in the presence of the corresponding dye. We conclude that inner weekly layers are 450-800 nm, and, taking into account 13 μm thickness of mature spicules (Veynberg, 2009), this corresponds to 2-3.5 months needed for complete maturation of the *L. baicalensis* spicules. This is a very rough estimation for several reasons: the growth rate possibly depends on the spicule age; fluorescent dye is possibly accumulated in the primmorph bodies and in sclerocytes, which lengthens the weekly interval of the dye change; the rate of spicule growth in natural sponges may differ from that in primmorphs. At the same time, long-time experiments with living *L. baicalensis* are impossible due to poor viability of the sponges in aquariums, and it is difficult to distinguish between such stages as a healthy sponge, an oppressed sponge or the onset of sponge cell atrophy. 3.5-6.5 monthly estimates of the growth of the spicules in primmorphs seem to be realistic since in experiments with different dyes we observed only a few 8-10 μm stained spicules after four months of primmorph cultivation.

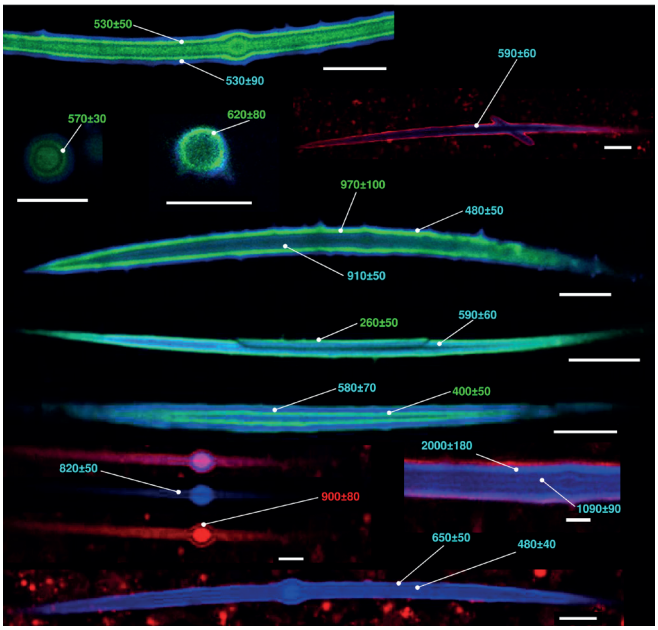

Fig. 11. Representative confocal microscopy images of *L. baicalensis* spicules stained with two dyes that were changed weekly during 4 months of primmorph cultivation. Green fluorescence - NBD-N2, blue - Q-N2 and red - Rhod-N3. Numbers correspond to the thickness of the stained layer, nm. Scale bars correspond to 10 μm.

4. Conclusions

Thus, new fluorescent dyes Q-N2 and Rhod-N3 are effective in vital staining of the growing siliceous spicules in sponge primmorphs. Cultivation of the sponge in the presence of these dyes allows for the use of confocal microscopy to study the morphology of the spicules and, in the case of two-color staining, to draw some conclusions about the growth rate of the spicules.

Acknowledgments

This work was supported by the Russian Academy of Sciences (project # AAAA-A19-119100490016-4). The authors thank the Center of Ultramicroanalysis (Limnological Institute) and Isotope-geochemical research center for Collective Use (A. P.Vinogradov Institute of Geochemistry of the Siberian Branch of the Russian Academy of Sciences) for providing equipment. We are deeply grateful to I. Khanaev for sponge samples and T. Avezova for measuring the toxicity of Rhod-N3.

References

Annenkov V.V., Danilovtseva E.N., Zelinskiy S.N. et al. 2010. Novel fluorescent dyes based on oligopropylamines for the in vivo staining of eukaryotic unicellular algae. Analytical Biochemistry 407: 44-51. DOI: 10.1016/j.ab.2010.07.032

Annenkov V.V., Glyzina O.Yu., Verkhozina O.N. et al. 2014. Fluorescent amines as a new tool for study of siliceous sponges. Silicon 6: 227-231. DOI: 10.1007/s12633-014-9220-4

Annenkov V.V., Pyshnyj D.V., Danilovtseva E.N. et al. 2016a. Analogues of natural deoxyribonucleoside triphosphates and ribonucleoside triphosphates containing reporter fluorescent groups, for use in analytical bioorganic chemistry. Patent RU 2582198

Annenkov V.V., Danilovtseva E.N. 2016b. Spiculogenesis in the siliceous sponge *Lubomirskia baicalensis* studied with fluorescent staining. Journal of Structural Biology 194: 29-37. DOI: 10.1016/j.jsb.2016.01.010

Annenkov V.V., Zelinskiy S.N., Pal'shin V.A. et al. 2019. Coumarin based fluorescent dye for monitoring of siliceous structures in living organisms. Dyes and Pigments 160: 336-343. DOI: 10.1016/j.dyepig.2018.08.020

Blunt J.W., Carroll A.R., Copp B.R. et al. 2018. Marine natural products. Natural Product Reports 35: 8-53. DOI: 10.1039/c7np00052a

Carroll A.R., Copp B.R., Davis R.A. et al. 2019. Marine natural products. Natural Product Reports 36: 122-173. DOI: 10.1039/c8np00092a

Custodio M.R., Prokic I., Steffen R. et al. 1998. Primmorphs generated from dissociated cells of the sponge *Suberites domuncula*: a model system for studies of cell proliferation and cell death. Mechanisms of Ageing and Development 105: 45-59. DOI: 10.1016/S0047-6374(98)00078-5

Denikina N.N., Dzyuba E.V., Bel'kova N.L. et al. 2016. The first case of disease of the sponge *Lubomirskia baicalensis*: investigation of its microbiome. Biology Bulletin 43: 263-270. DOI: 10.1134/S106235901603002X

El-Demerdash A., Atanasov A.G., Horbanczuk O.K. et al. 2019. Chemical diversity and biological activities of marine sponges of the Genus *Suberea*: A systematic review. Marine Drugs 17: 115. DOI: 10.3390/md17020115

Khalifa S.A.M., Elias N., Farag M.A. et al. 2019. Marine natural products: a source of novel anticancer drugs. Marine Drugs 17: 491. DOI: 10.3390/md17090491

Khanaev I.V., Kravtsova L.S., Maikova O.O. et al. 2018. Current state of the sponge fauna (Porifera: Lubomirskiidae) of Lake Baikal: sponge disease and the problem of conservation of diversity. Journal of Great Lakes Research 44: 77-85. DOI: 10.1016/j.jglr.2017.10.004

Kwon J.Y., Jang Y.J., Lee Y.J. et al. 2005. A highly selective fluorescent chemosensor for Pb^{2+}. Journal of the American Chemical Society 127: 10107-10111. DOI:

10.1021/ja051075b

Mcheik A., Cassaignon S., Livage J. et al. 2018. Optical properties of nanostructured silica structures from marine organisms. Frontiers in Marine Science 5: 123. DOI: 10.3389/fmars.2018.00123

Taylor M.W., Radax R., Steger D. et al. 2007. Sponge-associated microorganisms: evolution, ecology, and biotechnological potential. Microbiology and Molecular Biology Reviews 71: 295-347. DOI: 10.1128/MMBR.00040-06

Veynberg E. 2009. Fossil sponge fauna in Lake Baikal region. In: Müller W.E.G., Grachev M.A. (Eds.), Biosilica in Evolution, Morphogenesis, and Nanobiotechnology. Berlin, Heidelberg, pp. 185-203. DOI: 10.1007/978-3-540-88552-8

Wilson H.V., 1907. On some phenomena of coalescence and regeneration in sponges. Journal of Experimental Zoology 5: 245-257. DOI: 10.1002/jez.1400050204.

Zhang Y.Q, Reed B.W., Chung F.R. et al. 2016. Mesoscale elastic properties of marine sponge spicules. Journal of Structural Biology 193: 67-74. DOI: 10.1016/j.jsb.2015.11.009

Zvereva Y., Medvezhonkova O., Naumova T. et al. 2019. Variation of sponge-inhabiting infauna with the state of health of the sponge *Lubomirskia baikalensis* (Pallas, 1776) in Lake Baikal. Limnology 20: 267-277. DOI: 10.1007/s10201-019-00576-0

Limnology and Freshwater Biology 2019 (5): 308-311 DOI:10.31951/2658-3518-2019-A-5-308

Short communication

ISSN 2658-3518
LIMNOLOGY FRESHWATER BIOLOGY
www.limnolfwbiol.com

Structure features and structural transformations of the maxillary bones in the Baikal cottoid fish

Tolmacheva Yu.P.*, Bun M.M.

Limnological Institute, Siberian Branch of the Russian Academy of Sciences, Ulan-Batorskaya Str., 3, Irkutsk, 664033, Russia

ABSTRACT. In this paper, we study morphogeometric parameters and histostructure of maxillary bones in three coastal Baikal Cottoidei species belonging to different trophic groups. The results of the study revealed that the main trend in the transition from benthography to ichthyography is the sequential elongation of jaws and reduction in the mouth thrust accompanied by a consistent change in the form and internal structure of bone elements. A detailed analysis of data revealed that the changes mostly concern additional morphological structures (processes) of the bones directly connected with musculoligamentous apparatus and experiencing the highest tension during the functioning of the maxillary system. The distinctive features of the structural transformations maxillary bones in different fishes is a consequence of the uneven effect of power load that changes when the body adapts to certain habitat conditions.

Keywords: cottoid fish, maxillary apparatus, morphogeometric parameters, histostructure, structural adaptation, external power load

Introduction

The study of trophic adaptations in Baikal fish represents a bulk of closely related species. This is very interesting due to the peculiarities of the Baikal ecosystem owing to its age and diversity of underwater landscapes. The cottoid group, whose representatives occupy at present practically all biotopes and trophic niches of the lake, has a special status amongst the Baikal fish. Three species of the family Cottidae, *Paracottus knerii*, *Leocottus kesslerii* and *Batrachocottus baicalensis* (Taliev, 1955; Sideleva, 2003), inhabit the littoral zone (from the water edge up to the depths of 250–300 m). The study of dietary habits within this biotopical group revealed two main trends of trophic adaptation, allowing these species to coexist in a single biotope: zoophagy and zoophagy + ichthyophagy (Taliev, 1955; Sideleva and Mekhanikova, 1990; Sideleva, 2003; Dzyuba, 2004; Miyasaka et al., 2006; Tolmacheva, 2008). Each species formed its morphofunctional features in the structure of the anterior digestive system as a result of adaptation to a specific trophic behavior (Taliev, 1955; Yabe, 1985; Sideleva and Mekhanikova, 1990; Sideleva, 2003; Tolmacheva, 2010). As any change in the function and structure of the system is followed, above all, by certain changes in its separate parts, it is relevant to apply the detailed approach to study latent regularities of these structural transformations in the closely related species of fish.

The present paper concerns a comparative morphometric and histological study of the maxillary bones and analysis of potential causes of their structural transformations in the Baikal cottoid fish from various trophic groups.

Materials and research methods

Osteological specimens of the maxillary bones of three species of cottoid fish from the Baikal littoral zone, *Paracottus knerii* (Dyb., 1874), *Leocottus kesslerii* (Dyb., 1874) and *Batrachocottus baicalensis,* were used in this study. Thirty specimens of each species were examined in total.

The standard methods for osteological analysis were used to study the shape of the maxillary bones (Standard methods…. 1976). The soft tissues were removed from the fish skulls with a 10% solution of NaOCl; the cleaned bones were stored in glycerol. The comparative analysis included 16 measurements (% of the bone length) of the anguloarticulare, dentale and praemaxillare. The method for constructing allometric networks similar to the approach used previously in analyzing the variability of the body shape of fish (Strauss and Bookstein, 1982; Strauss and Fuiman, 1985; Tolmacheva, 2011) was used to create geometric structures of the maxillary bones. The geometric design was performed via the Autocad 2010 software (http://www.autodesk.ru) (Fig. 1).

*Corresponding author.
E-mail address: tjul78@mail.ru (Yu.P. Tolmacheva)

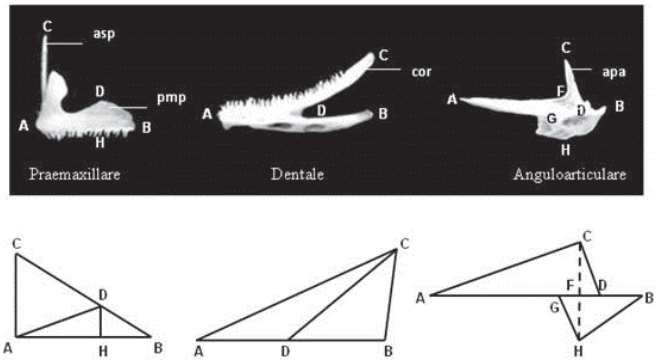

Fig. 1. The construction scheme of morphogeometric design of the maxillary bones in cottoid fish: a) the measurement scheme in osteological analysis; b) projection of measurements (in % of bone length) in morphgeometric design. Legend: Praemaxillare: asp – pmx ascending process, pmp – pmx maxillary process, (AC – asp height, AH – pmp location, DH – pmp height); Dentale: cor – den coronoid process (BC den height, AC – location of the cor posterior end, DC – cor length, BD – den notch depth); Articulare: apa – superior art process (CH – art height, AD – location of suprascapular notch (base of superior process), CD – height of superior process, CF – location of superior process: AG – location of inferior notch).

The histological structures of the maxillary tissues were studied according to the standard methods (Merkulov, 1969). The material was fixed in a 10% buffer formalin solution, which was decalcified with a 5% nitric acid solution and put into wax-paraffin. The 10-μm thick sections were stained with hematoxylin-eosin. The anatomical structure of each bone was presented as longitudinal and transverse sections. Morphometric analysis of the specimens was performed using a binocular light microscope (S. Zeiss) and ImageScope Color Image Analysis software (Moscow, 2008). The following parameters were chosen for the analysis: bone area, cartilage and bone cavity (thousand μm^2/area of one field of view). The average area of one field of view was 1.73 μm^2 at 125-fold magnification. Each specimen was analyzed in 10 areas of view.

Results and disscusion

The objects studied were closely related species of cottoid fish that inhabit the littoral zone of Lake Baikal and have a similar feeding behavior. The previous investigations of the maxillary apparatus of these fish revealed the growth of its linear parameters in the following direction: *Paracottus knerii - Leocottus kesslerii - Batrachocottus baicalensis*. This was due to the consumption of prey with different size and incomplete transition to ichthyophagy (Tolmacheva, 2010) (Fig. 2).

Morphogeometrical parameters. The morphometric analysis together with a geometric approach made the set of linear measurements more illustrative and enabled to investigate the simple regularities that are not always apparent without visualization (Fig. 2):

Upper jaw (*praemaxillare* + *maxillare*). Elongation of the upper jaw is followed by a consistent reduction of its ascending process of *praemaxillare.* This is often observed in other fish species. The relative height of the ascending process in the zoophage *P. knerii* and *L. kesllerii* was 81% and 70%, respectively, of the *praemaxillare* length, whereas it was 52% in the facultative ichthyophage *B. baicalensis*.

Lower jaw *(dentale* + *anguloarticulare)*. The main differences in the relative parameters of the lower jaw amongst the studied species are limited to the reduction of the bone height. The relative height of the *dentale* in *P. knerii* and *L. kesllerii* was 41.6 and 43%, respectively, and 35% – in *B. baicalensis*. It is noteworthy that the *anterior process* of *anguloarticulare* is consistently retracted (70%, 77% and 71% in *P. knerii, L. kesllerii and B. baicalensis*, respectively) and dislocated in a more horizontal position (Fig. 2). The anterior process (70 - 71%) and the lower process (62%) remain in unaltered position.

The measurements show that the consistent elongation of the jaw and reduction of the mouth protrusion in the studied species is followed by an appropriate change in mouth shape and the ratio of its morphological structures (Taliev, 1955; Sideleva and Mekhanikova, 1990; Sideleva, 2003; Tolmacheva, 2008; 2010). The power load, which changed during evolution, is the main factor that affects the morphogenesis of the bone tissue (Wolff, 1892). Hence, a transformation of the bone shape should primarily occur in the regions of the maximum stress during the functioning of the maxillary apparatus.

The protrusion of the upper jaw in the cottoid fish results from gliding the ascending processes of *praemaxillare* along the *ethmoideum*. The degree of the protrusion depends on two interdependent features: the length of the *praemaxillare* and the height of the ascending process (Gregory, 1933; O'Kamura, 1970; Voskoboinikova, 1986). The ascending processes of *praemaxillare* carry the maximum power load, resulting

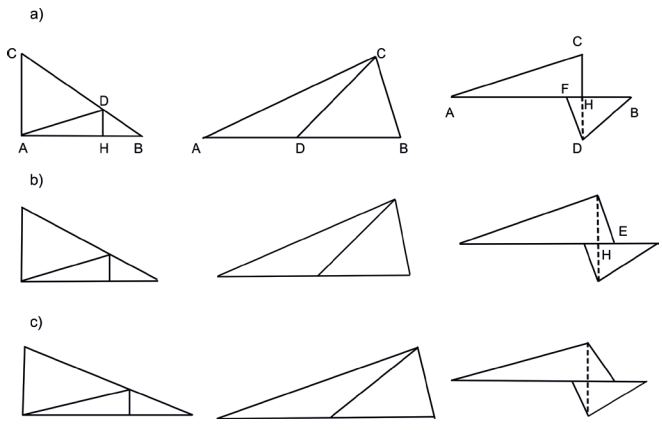

Fig. 2. Morphogeometric design of jaw apparatus bones in littoral species of Cottoidei belonging to diffirenent trophic groups: a) *Paracottus knerii; b)Leocottus kesslerii; c) Batrachocottus baicalensis.*

from the functioning of the maxillary apparatus in the anamniotes (Lebedkina, 1980). An elongation of the *praemaxillare* in ichthyophages significantly increases the pressure on the ascending processes and, thus, leads to their gradual reduction.

The lesser degree of protrusion requires more efforts to close the mouth (Aleev, 1963). This process is carried out with the *musculus adductor mandibulae* (A2, A3 and AW), whose portions are predominantly attached to the internal side of the *anguloarticulare* and the anterior process (Dobben, 1935; Yabe, 1985). The transformation of the *anguloarticulare* shape and the consistent dislocation of the anterior process in a horizontal plane is due to the increasing power stress from the muscles. In turn, the dislocation of the anterior process of *anguloarticulare* in a horizontal plane reduces the *dentale* that contacts with it in the region of the coronoid process.

Histostructure. The histological analysis shows that rough fibrous tissue typical of the bony fish represents the microstructure of maxillary bones in the studied species (Meunier and Desse, 1986). There are compacted portions of cartilaginoid tissue in the contact areas. The surface of each bone represents a compact structure above bone cavities that are connected by anastomoses and form a single network (Fig. 3a). Inside the cavities, there are fragments of osteoblasts that were destroyed during the preparation of the specimens.

The number and size of the cavities significantly vary within the same bone (Fig. 3a, Fig. 3b). E.g., many small cavities, making 30-43% of the total area in a vertical section of the bone, represent the network structure inside the bones. The internal structure of the processes (*ascending process of praemaxillare, anterior process of anguloarticulare* and *coronoid process of dentale*) represent a single large cavity (50-69% in area) that is encircled by a layer of a dense coarse fibrous tissue.

Bias in the external mechanical load on the formation of the bone tissue induces the heterogeneity of the network structure (the bone cavities become fewer and larger) in different portions of the same bone. In the study of the internal structure of the maxillary apparatus in the Scaridae, the area of the cavities increased in the region of the maximum stress (Bogachik, 1999). We determined this regularity in the microstructure of the processes of the maxillary bones that are the most affected by the muscular-ligamentous apparatus.

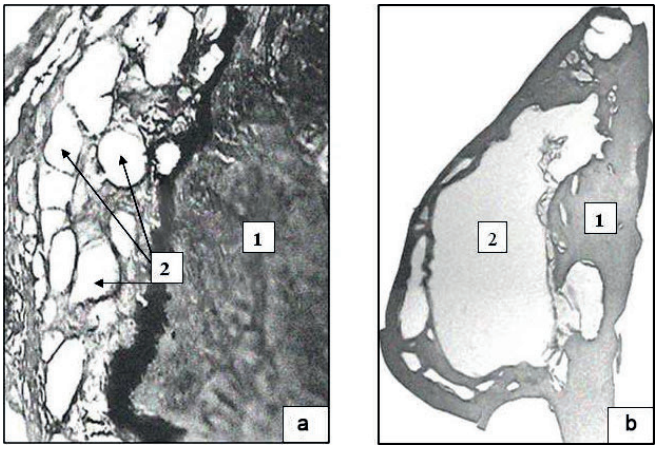

Fig. 3. Anguloarticulare histostructure of the bighead sculpin *Batrachocottus baicalensis*: a) transverse section of the bone; b) transverse section of the anguloarticulare superior process. 1 – compact tissue, 2 – medulary cavities. Magnification x125.

Conclusion

Thus, changes in functional requirements in a specific environment cause the adaptive transformations of the maxillary apparatus of the fish. The main trend observed in the Baikal cottoid fish at the transition from benthos feeding to ichthyophagy is a consistent elongation of the jaw and reduction of the upper jaw protrusion followed by an appropriate change in the shape, size and internal structure of the main bone elements. The transformation of the bone shape and internal structure occurs in the regions of the maximum stress that occurs during the functioning of the maxillary apparatus. It mainly concerns supplementary elements (processes) of the maxillary bones that are directly connected to the muscular-ligamentous apparatus and most exposed to external forces. Overall, the peculiarities of the structural transformations of the maxillary system in different species is a result of uneven power load that changes during adaptation of an organism to a specific environment.

Acknowledgements

The work was performed within the project No. 0345–2019–0002.

References

Aleev Yu.G. 1963. Funktsional'nyye osnovy vneshnego stroyeniya ryb. Moscow: Publishing House of the USSR Academy of Sciences. (in Russian)

Bogachik T.A. 1999. Histological analysis of the microstructure of the jaw and pharyngeal apparatus of two species of scar fish (Scaridae). In: Lobkov V.A. (Ed.), Razvitiye zoologicheskikh issledovaniy v Odesskom universitete. Odessa, pp. 163-174. (in Russian)

Dobben W.N. 1935. Uber der Kiefermechanismus der Knochenfishe. Archives Néerlandaises de Zoologie [Dutch Archives of Zoology] 50: 1-72. (in German)

Dzyuba E.V. 2004. Issledovaniye pishchevykh strategiy pelagicheskikh ryb Baykala. Cand. Sc. Dissertation, Papanin Institute for Biology of Inland Waters RAS, Borok, Russia. (in Russian)

Gregory W.K. 1933. Fish skulls. A study of the evolution of natural mechanism. Transactions of the American Philosophical Society 23: 75-481.

Lebedkina N.S. 1980. Leading traits in phylogenetics. In: Morfologicheskiye aspekty evolyucii. Moscow, pp. 53-64. (in Russian)

Merkulov G.A. 1969. Kurs patogistologicheskoy tekhniki. Leningrad: Meditsyna. (in Russian)

Meunier F.J., Desse G. 1986. Les hyperostose les Téléostéens: description, histolog et problémes étiologique. Ichthyophysiological Acta 10: 130-141. (in French)

Miyasaka H., Dzyuba Ye.V., Genkai-Kato M. et al. 2006. Feeding ecology of two planktonic sculpins, *Comephorus baicalensis* and *Comephorus dybowskii* (Comephoridae), in Lake Baikal. Ichthyological Research 53: 419-422.

O'Kamura O. 1970. Studies of the Macrouroid fishes of Japan. Morphology, ecology and phylogeny. Reports of the USA Marine Biological Station 17: 33.

Sideleva V.G. 2003. The endemic fishes of Lake Baikal. Leiden: Backhuys Publ.

Sideleva V.G., Mechanikova I.V. 1990. Food specialization and evolution of bullhead fish (Cottoidei) in Lake Baikal. Trudy Zoologicheskogo Instituta [Proceedings of Zoological Institute of the USSR Academy of Sciences] 222: 144-161. (in Russian)

Tipovyye metodiki issledovaniya produktivnosti vidov ryb v predelakh ikh arealov. 1976. Vilnius: Moxlas. (in Russian)

Strauss R., Bookstein F.L. 1982. The truss: body form reconstructions in morphometrics. Systematic Zoology 31: 113-135. DOI: 10.1093/sysbio/31.2.113

Strauss R., Fuiman L. 1985. Quantitative comparisons of body form and allometry in larval and adult Pacific sculpins (Teleostei: Cottidae). Canadian Journal of Zoology 63: 1582-1589. DOI: 10.1139/z85-234

Taliev D.N. 1955. Bychki-podkamenshchiki Baykala. Moscow-Leningrad: Publishing House of the USSR Academy of Sciences. (in Russian)

Tolmacheva Yu.P. 2008. Comparative characteristic of feeding of three species of cottoidei in the littoral of southern Baikal (Cape Berezovyi). Journal of Ichthyology 48: 499-504. DOI: 10.1134/S0032945208070035

Tolmacheva Yu.P. 2010. Structure of the mouth opening and pharyngeal apparatus in three species of Baikal Cottoidei in relation to their feeding. Journal of Ichthyology 50: 65-72. DOI: 10.1134/S003294521001l008X

Tolmacheva Yu.P. 2011. Geometricheskaya konstruktsiya v issledovanii stroyeniya chelyustnogo apparata ryb. In: 1st International Scientific-Practical Conference "Sovremennyye Zoologicheskiye Issledovaniya v Rossii i Sopredel'nykh Stranakh" ["Modern Zoological Research in Russia and Neighboring Countries"], pp. 138-142. (in Russian)

Voskoboinikova O.S. 1986. Evolutionary transformations of the visceral skeleton and phylogeny issues of nototheniidae fish (Nototheniidae). Trudy Zoologicheskogo Instituta [Proceedings of Zoological Institute of the USSR Academy of Sciences] 153: 46-66. (in Russian)

Wolff J. 1892. Das Gesetz der Transfomation der Knochen. Berlin: Hirshwald. (in German)

Yabe M. 1985. Comparative osteology and miology of the superfamily Cottoidea (Pisces: Scorpaeniformes), and its philogenetic classification. Memoirs of the Faculty of Fisheries Hokkaido University 32: 1-130.

Limnology and Freshwater Biology 2019 (5): 312-315 DOI:10.31951/2658-3518-2019-A-5-312

Short communication

ISSN 2658-3518
LIMNOLOGY FRESHWATER BIOLOGY
www.limnolfwbiol.com

Evaluation of water suspension effect on spectral light attenuation in Novosibirsk Reservoir

Akulova O.B.*, Bukaty V.I.

Institute for Water and Environmental Problems SB RAS, Molodezhnaya St., 1, Barnaul, Altai Krai, 656038, Russia

ABSTRACT. The paper presents the measurement data (August 20 – 22, 2019) on spectral light attenuation in the Novosibirsk Reservoir waters in the range from 400 to 800 nm. In different sampling stations, attenuation (calculated on the natural logarithmic base) varied within 4.6 – 25.9 m^{-1}. Relative transparency (42 – 140 cm) was measured using a Secchi disk. To assess the effect of water suspension on total attenuation, we calculated its relative spectral contribution and other main optically active components of water, i.e. yellow substance, chlorophyll *a* and pure water. Yellow substance and suspension showed the maximum contribution to light attenuation in the water from all 10 sampling stations of the reservoir. The spectral contribution of suspension was 30 – 60% in the range of 430 nm, 39 – 71% at 550 nm and 33 – 64% at 670 nm, respectively. The suspension was the second optically active component affecting spectral light attenuation.

Keywords: spectral light attenuation coefficient, suspension, yellow substance, chlorophyll *a*, pure water, Novosibirsk Reservoir

1. Introduction

Water suspension is one of the most important optically active components of any natural or manmade water body. Along with yellow substance (YS), chlorophyll *a* and pure water, suspension has a significant effect on total light attenuation (Kopelevich, 1983; Reinart et al., 2004; Mankovsky and Sherstyankin, 2007; Mankovsky, 2011; Onderka et al., 2011; Shuchman et al., 2013; Levin, 2014; Korosov et al., 2017; Shi et al., 2017; Churilova et al., 2018). Therefore, its optical characteristics dependent on particles' size, quantity, material, shape and orientation require a thorough study. Water suspension is often understood as a set of large (with a diameter of 0.5 μm to 1 mm), small (0.45 – 1 μm) and colloidal (0.001 – 0.1 μm) particles, which consist of terrigenous (mineral) and biological (organic) fractions (Clavano et al., 2007). The relationship between suspended substance concentrations and spectral light attenuation directly depends on the composition and properties of suspension, namely, a size, a shape and a refractive index of particles. All this determines the regional features of the water body under study.

The aim of this work is to evaluate the water suspension effect on spectral light attenuation based on the calculated experimental data, i.e. the relative spectral contribution of main optically active water components of the Novosibirsk Reservoir waters in the summer of 2019.

2. Material and methods

The study object is Novosibirsk Reservoir; by the water area, it is the largest (regardless of the Irtysh) in the Ob River basin manmade reservoir constructed for the multipurpose use, i.e. water supply (mainly drinking water), hydropower, irrigation, fish farming, and recreation. The results of 10 processed and analyzed water samples taken by a bathometer from the surface water layer of Novosibirsk Reservoir became the basis for our study. For observations on August 20 – 22, 2019, we used a research vessel. Table 1 shows numbers, names and coordinates of sampling stations.

Hydro-optical characteristics of water samples were measured in the laboratory using a single-beam spectrophotometer PE-5400UF operating in the mode of measuring spectral water transparency (transmittance) with further calculations of spectral light attenuation $\varepsilon(\lambda)$ in the wavelength range of 400 – 800 nm with a step of 30 nm. Spectral light absorption by yellow substance $\kappa_{ys}(\lambda)$ was defined after measuring spectral transparency of the water purified from suspension by filtration through the «Vladipor» type MFAS-OS-1 membranes with a pore diameter of 0.22 μm. Overall, 240 measurements of spectral water transparency were carried out. The $\varepsilon(\lambda)$ (at the natural logarithmic base) value was calculated according to the formula

$$\varepsilon(\lambda) = (1/L) \cdot \ln(1/T(\lambda)) \qquad (1)$$

*Corresponding author.
E-mail address: akulova8282@mail.ru (O.B. Akulova)

derived from the Booger's law, where L is the cuvette length, $T(\lambda) = I(\lambda)/I_0(\lambda)$ – the transparency (transmittance) in relative units, $I(\lambda)$, $I_0(\lambda)$ – the intensity of transmitted and incident light, respectively, λ – the wavelength of light. The absolute error of $\varepsilon(\lambda)$ is induced by the spectrophotometer instrument error during transmittance measurement ($\Delta T = 0.5\%$) and the measurement error of a cuvette length. In the experiment, we used cuvettes with a length $L = 50$ mm. The maximum absolute error in defining the light attenuation coefficient was 0.1 m^{-1}.

The concentration of chlorophyll *a* in acetone extracts of phytoplankton algae was found through a standard spectrophotometric method according to the standard GOST 17.1.4.02-90. Relative transparency of *Z* was measured using a Secchi disk.

The relative spectral contribution of optically active components of water (suspension, yellow substance, chlorophyll and pure water) to $\varepsilon(\lambda)$ was calculated using a modified semi-empirical spectral model of light attenuation (Akulova, 2015), which was first proposed in Kopelevich, 1983, as follows:

$$\varepsilon(\lambda) = \kappa_{chl}(\lambda) + \kappa_{ys}(\lambda) + \sigma_{mol}(\lambda) + \sigma_s(\lambda) + \kappa_{pw}(\lambda) \quad (2)$$

where $\kappa_{chl}(\lambda)$ and $\kappa_{ys}(\lambda)$ – spectral absorption by chlorophyll and yellow substance, respectively, $\sigma_{mol}(\lambda)$ – spectral scattering by pure water, $\sigma_s(\lambda)$ – spectral dispersion by suspension, $\kappa_{pw}(\lambda)$ – spectral absorption by pure water. The calculated attenuation in the formula (1) does not contain the attenuation coefficient of pure water $\varepsilon_{pw}(\lambda) = \kappa_{pw}(\lambda) + \sigma_{mol}(\lambda)$. In the formula (2), we summed up the $\varepsilon(\lambda)$values obtained from spectrophotometer measurements with $\varepsilon_{pw}(\lambda)$ taken from the reference data (Kopelevich, 1983; Levin, 2014).

Rate of chlorophyll absorption was calculated as follows:

$$\kappa_{chl}(\lambda) = \kappa_{sp.chl}(\lambda) \cdot C_{chl} \quad (3)$$

Where C_{chl} is the concentration of chlorophyll *a*, mg/m^3, $\kappa_{sp.chl}(\lambda)$ – the specific chlorophyll absorption, m^2/mg (Kopelevich, 1983). For calculations of $\kappa_{pw}(\lambda)$, we used the tabular data of Levin (2014), whereas for $\sigma_{mol}(\lambda)$ – Kopelevich (1983).

According to the expression (2), spectral light attenuation is described via a three-parameter model. In contrast to the previous studies (where parameter $\sigma_s(\lambda)$ is determined experimentally, and $\kappa_{ys}(\lambda)$ is the difference between the measured $\varepsilon(\lambda)$ and the sum of other parameters), we propose an alternative approach. Since the $\kappa_{ys}(\lambda)$ parameter was identified experimentally, spectral scattering of suspension $\sigma_s(\lambda)$ can be found from the expression (2) with the following formula:

$$\sigma_s(\lambda) = \varepsilon(\lambda) - [\kappa_{chl}(\lambda) + \kappa_{ys}(\lambda) + \sigma_{mol}(\lambda) + \kappa_{pw}(\lambda)] \quad (4)$$

3. Results and discussion

Hydro-optical characteristics (spectral parameters of light attenuation $\varepsilon(\lambda)$ and light absorption by yellow substance $\kappa_{ys}(\lambda)$ as well as relative transparency *Z* in the surface layer of the water differed significantly during the study period. The spectral light attenuation coefficient made up 4.6 – 25.9 m^{-1} within 400 – 800 nm (August 20 – 22, 2019). For instance, $\varepsilon(\lambda)$ varied as 10.9 – 22.4 m^{-1} at the wavelength $\lambda = 430$ nm, 7.0 – 15.9 m^{-1} at $\lambda = 550$ nm and 5.7 – 12.7 m^{-1} at $\lambda = 670$ nm. These wavelengths were chosen because maximal light absorption by chlorophyll fell on $\lambda = 430$ and 670 nm, whereas the greatest solar radiation – at $\lambda = 550$ nm, which was taken into account under optical device development and used as a marker in hydro-optical studies.

Relative transparency *Z* measured using a Secchi disk was in the range of 42 – 140 cm. Its maximum was recorded on the right bank of the Leninskoye–Sosnovka section (station 7.3).

Table 1. Sampling stations and their coordinates in the surface layer of Novosibirsk Reservoir (August 2019)

Sampling date	Station number (name)	Coordinates
20.08.2019	1.2 (Kamen-on-Ob, a midpoint of the reservoir section)	53.4629932 N 81.2320987 E
21.08.2019	3.2 (Maletino, a midpoint of the reservoir section)	54.0253884 N 81.2435273 E
21.08.2019	4.2 (Spirino, a midpoint of the reservoir section)	54.0738719 N 81.3344964 E
21.08.2019	5.1 (Ordynskoye–Nizhnekamenka, left bank)	54.2112316 N 81.5434117 E
21.08.2019	5.3 (Ordynskoye–Nizhnekamenka, right bank)	54.1926605 N 81.5436392 E
22.08.2019	6.3 (Borovoye–Bystrovka, right bank)	54.3352643 N 82.3308600 E
22.08.2019	7.3 (Leninskoye–Sosnovka, right bank)	54.4108884 N 82.5331697 E
22.08.2019	8.2 (Berdsky gulf, Agroles, a midpoint of the reservoir section)	54.4554623 N 83.90216 E
22.08.2019	9.2 (Berdsky gulf, Rechkunovka, a midpoint of the reservoir section)	54.4735297 N 83.0420651 E
22.08.2019	10.2 (head reach, near the HPP dam)	54.4954354 N 82.5811518 E

Table 2. Spectral contribution of water components (%) to light attenuation in the surface layer of Novosibirsk Reservoir (August 20 – 22, 2019)

Wavelength of light λ, nm	Light absorption			Light scattering	Light attenuation ε, m^{-1}
	$\frac{\kappa_{pw}(\lambda)}{\varepsilon(\lambda)}$	$\frac{\kappa_{ys}(\lambda)}{\varepsilon(\lambda)}$	$\frac{\kappa_{chl}(\lambda)}{\varepsilon(\lambda)}$	$\frac{\sigma_s(\lambda)+\sigma_{mol}(\lambda)}{\varepsilon(\lambda)}$	
station 1.2 (C_a = 17.6 mg/m^3)					
430	0.1	55.3	8.3	36.3	16.8
550	0.5	42.8	0.9	55.8	11.9
670	4.6	39.3	7.4	48.7	9.4
station 3.2 (C_a = 16.9 mg/m^3)					
430	0.1	50.3	9.4	40.2	14.3
550	0.5	42.3	1.0	56.2	10.4
670	5.0	39.5	7.8	47.7	8.6
station 4.2 (C_a = 18.7 mg/m^3)					
430	0.1	33.0	6.6	60.3	22.4
550	0.3	27.6	0.7	71.4	15.9
670	3.4	26.7	5.8	64.1	12.7
station 5.1 (C_a = 8.7 mg/m^3)					
430	0.1	58.1	4.3	37.5	16.0
550	0.5	44.7	0.5	54.3	11.4
670	4.6	38.3	3.7	53.4	9.4
station 5.3 (C_a = 10.5 mg/m^3)					
430	0.1	38.5	4.7	56.7	17.9
550	0.4	33.0	0.5	66.1	13.0
670	4.1	31.7	4.0	60.2	10.4
station 6.3 (C_a = 6.7 mg/m^3)					
430	0.1	41.2	2.9	55.8	18.2
550	0.5	38.2	0.4	60.9	11.5
670	4.8	37.0	3.0	55.2	8.9
station 7.3 (C_a = 6.4 mg/m^3)					
430	0.1	58.7	4.0	37.2	12.6
550	0.6	51.2	0.5	47.7	8.2
670	6.7	49.2	3.9	40.2	6.5
station 8.2 (C_a = 13.5 mg/m^3)					
430	0.1	49.3	6.7	43.9	16.0
550	0.5	43.3	0.8	55.4	10.6
670	5.0	40.6	6.3	48.1	8.6
station 9.2 (C_a = 10.1 mg/m^3)					
430	0.1	60.6	4.9	34.4	16.5
550	0.5	51.4	0.6	47.5	10.3
670	5.5	44.3	5.1	45.1	7.9
station 10.2 (C_a = 4.4 mg/m^3)					
430	0.1	66.9	3.2	29.8	10.9
550	0.8	60.0	0.4	38.8	7.0
670	7.6	56.1	3.1	33.2	5.7

The calculated concentrations of chlorophyll *a* in the surface layer of Novosibirsk Reservoir were within 4.4 – 18.7 mg/m^3, with an average of 11.3 mg/m^3. Based on the long-term data, spatial heterogeneity of the chlorophyll content was studied thoroughly in the Laboratory of Aquatic Ecology of IWEP SB RAS (Kotovshchikov, 2018).

Table 2 presents the calculation results of the spectral contribution of the main optically active components of water (suspension, yellow substance, chlorophyll *a*, and pure water) to spectral light attenuation $\varepsilon(\lambda)$ in various sampling stations of Novosibirsk Reservoir. Here, values $\varepsilon(\lambda)$ and $\kappa_{ys}(\lambda)$ are given on the natural logarithmic base.

The result of calculations of relative spectral contribution of optically active water components to light attenuation $\varepsilon(\lambda)$ in the surface layer of Novosibirsk Reservoir in various sampling stations suggests that yellow substance and suspension have the greatest optical effect on total attenuation. The calculations show that yellow substance provides the greatest contribution (67%) to light attenuation at λ = 430

nm in the upper reach, nearby the HPP dam (station 10.2). At other sampling stations, the contribution of YS varies within 33 – 61%. At $\lambda = 550$ nm, the relative contribution of YS ranges from 28% (station 4.2 – Spirino, a midpoint of the reservoir section) to 60% (station 10.2); at $\lambda = 670$ nm, the HPP dam has the largest YS contribution (56%). The maximum suspension contribution (over 60%) is observed at the station 4.2 (Spirino, a midpoint of the reservoir section) at $\lambda = 430$ nm, with its increase up to 71% at $\lambda = 550$ nm. At $\lambda = 670$ nm, the suspension contribution varies from 33% (station 10.2) to 64% (station 4.2). Pure water makes an insignificant contribution (less than 0.1%) to light attenuation at $\lambda = 430$ nm at all stations. However, it increases sharply (8%) at $\lambda = 670$ nm. The contribution of chlorophyll at $\lambda = 430$ nm reaches from 3% (station 6.3 – Borovoye–Bystrovka, right bank) to 9% (3.2 – Maletino, a midpoint of the reservoir section); at $\lambda = 550$ nm it is from 0.4% (stations 6.3 and 10.2) to 1% (3.2). At $\lambda = 670$ nm, the maximum chlorophyll contribution is observed at station 3.2 (8%). Molecular light scattering by pure water in the studied spectral range is responsible for a small contribution (0.1%).

Thus, suspension in waters of Novosibirsk Reservoir is the second most important optically active component affecting spectral light attenuation.

4. Conclusion

The article presents the optical experiment results for assessing water suspension effect on spectral light attenuation obtained during the implementation of a series of complex hydrological studies in the water area of Novosibirsk Reservoir in August 2019. Being one of the most optically active water components able to affect light attenuation (under certain physicochemical conditions), the suspension may serve as an important indicator of water quality. Therefore, further research is of particular importance.

Acknowledgments

We express our gratitude to Kotovschikov A.V., a senior researcher of the Laboratory of Hydrobiology, IWEP SB RAS for water sampling and the provided measuring data on chlorophyll *a* and relative transparency determined using a Secchi disk.

The work was carried out within the framework of the Research Program of IWEP SB RAS (project No. AAAAA 17-117041210241-4).

References

Akulova O.B. 2015. Development of methods and a measuring computer system for assessing ecologically significant hydro-optical characteristics of freshwater reservoirs (by the example of lakes in Altai Krai). Cand. Sc. Dissertation, Institute for Water and Environmental Problems SB RAS, Barnaul, Russia. (in Russian)

Churilova T.Ya., Moiseeva N.A., Latushkin A.A. et al. 2018. Preliminary results of bio-optical investigations at Lake Baikal. Limnology and Freshwater Biology 1: 58-61. DOI: 10.31951/2658-3518-2018-A-1-58

Clavano W.R., Boss E., Karp-Boss L. 2007. Inherent optical properties of non-spherical marine-like particles – from theory to observation. Oceanography and Marine Biology: An Annual Review 45: 1-38.

Kopelevich O.V. 1983. A low-parameter model of the optical properties of sea water. In: Monin A.S. (Ed.), Optika okeana. T.1. Fizicheskaya optika okeana. Moscow, pp. 208-235. (in Russian)

Korosov A.A., Pozdnyakov D.V., Shuchman R. et al. 2017. Bio-optical retrieval algorithm for the optically shallow waters of Lake Michigan. I. Model description and sensitivity/ robustness assessment. Trudy Karel'skogo Nauchnogo Tsentra RAN [Transactions of the Karelian Research Centre of RAS] 3: 79-92. DOI: 10.17076/lim473 (in Russian)

Kotovshchikov A.V., Yanygina L.V. 2018. Spatial heterogeneity of chlorophyll *a* content in Novosibirsk reservoir. Izvestiya Altayskogo Otdeleniya Russkogo Geograficheskogo Obshchestva [Bulletin AB RGS] 3: 46-52. (in Russian)

Levin I.M. 2014. Low-parametric models of primary optical characteristics of sea water. Fundamental'naya i Prikladnaya Gidrofizika [Fundamental and Applied Hydrophysics] 7: 3-22. (in Russian)

Mankovsky V.I., Sherstyankin P.P. 2007. Spectral model of an indicator of directional light weakening in waters of Lake Baikal in summer. Morskoy Gidrofizicheskiy Zhurnal [Marine Hydrophysical Journal] 6: 39-46. (in Russian)

Mankovsky V.I. 2011. Spectral contribution of components of sea water to an indicator of directional light weakening in the surface water of the Mediterranean Sea. Morskoy Gidrofizicheskiy Zhurnal [Marine Hydrophysical Journal] 5: 14-29. (in Russian)

Onderka M., Rodný M., Velísková Y. 2011. Suspended particulate matter concentrations retrieved from self-calibrated multispectral satellite imagery. Journal of Hydrology and Hydromechanics 59: 251-261. DOI: 10.2478/ v10098-011-0021-9

Reinart A., Paavel B., Pierson D. et al. 2004. Inherent and apparent optical properties of Lake Peipsi, Estonia. Boreal Environment Research 9: 429-445.

Shi L., Mao Z., Wu J. et al. 2017. Variations in spectral absorption properties of phytoplankton, non-algal particles and chromophoric dissolved organic matter in Lake Qiandaohu. Water 9. DOI: 10.3390/w9050352

Shuchman R.A., Leshkevich G., Sayers M.J. et al. 2013. An algorithm to retrieve chlorophyll, dissolved organic carbon, and suspended minerals from Great Lakes satellite data. Journal of Great Lakes Research 32: 14-33. DOI: 10.1016/j. jglr.2013.06.017